

THESIS FOR THE DEGREE OF DOCTOR OF PHILOSOPHY

Heat control in mesoscopic conductors -
exploiting quantum effects and size confinement

FATEMEH HAJILOO

Department of Microtechnology and Nanoscience (MC2)

Applied Quantum Physics Laboratory

CHALMERS UNIVERSITY OF TECHNOLOGY

Göteborg, Sweden 2020

Heat control in mesoscopic conductors - exploiting quantum effects and size confinement

FATEMEH HAJILOO

Göteborg, Sweden 2020

ISBN 978-91-7905-409-0

COPYRIGHT © FATEMEH HAJILOO, 2020

Doktorsavhandlingar vid Chalmers tekniska högskola

Ny serie Nr 4876

ISSN 0346-718X

Applied Quantum Physics Laboratory

Department of Microtechnology and Nanoscience (MC2)

Chalmers University of Technology

SE-412 96 Göteborg, Sweden

Telephone: +46 (0)31-772 1000

Cover

Sketch of an artistic view of electronic heat transport through a temperature-biased junction.

Printed by Chalmers Reproservice

Göteborg, Sweden 2020

Heat control in mesoscopic conductors - exploiting quantum effects and size confinement

FATEMEH HAJILOO

Applied Quantum Physics Laboratory

Department of Microtechnology and Nanoscience (MC2)

Chalmers University of Technology

ABSTRACT

This thesis deals with a theoretical analysis of heat currents, their exploitation and their control in nanoscale devices. The motivation for this study is twofold. (i) The development of nanoscale devices sets up the basis of many applications ranging from nanoelectronics to quantum technology. Such nanodevices, typically operated at low temperatures, are highly sensitive to heating effects. Hence the successful performance of these devices relies on controlling and managing this heat. (ii) Nanostructures provide appealing systems to study quantum and nonequilibrium thermodynamics because, at such small scales, the behavior of systems is highly affected by size confinement and quantum effects.

The central purpose of this thesis is to investigate the impact of specific characteristics of quantum systems, in particular of quantum size confinement, nonequilibrium effects and phase coherence, on heat transport quantities. A better understanding of this impact can lead to an improved control and exploitation of heat. This can be used for the evacuation of heat from the system, cooling, or producing power using waste heat. We propose different experimentally accessible setups. In these setups, we theoretically study transport quantities using a scattering formalism.

We pursue three main study lines in different setups: (i) We investigate phase-dependent heat transport in normal- and superconducting hybrid junctions. We show how disorder influences this, both in simple junctions as well as in a heat circulator. (ii) We analyze thermodynamical machines, which use nonequilibrium states as their resource instead of heat. Such devices show a "demonic behavior" since they seemingly challenge the second law of thermodynamics. (iii) We analyze how to exploit energy filtering of quantum conductors to perform thermoelectric cooling at the example of a quantum spin Hall device in the whole range from linear to nonlinear response.

Keywords: heat currents; fluctuations; phase-dependent heat transport; thermoelectric devices; nonequilibrium thermodynamics.

ACKNOWLEDGEMENTS

I would like to express my sincere gratitude to Janine Splettstoesser, my supervisor, for her enthusiasm for the work, for her support and providing guidance and feedback throughout my Ph.D., for her encouragement and patience. I am grateful to thank my co-supervisor, Fabian Hassler, at RWTH Aachen University. I had a very productive time during my visit to Aachen, which all comes from your help. Thank you for encouraging my research and for your hospitality. It gives me great pleasure in acknowledging the support of my examiner, Göran Johansson.

I would like to extend my sincere thanks to our collaborators, Rafael Sánchez and Robert Whitney, for their insightful comments and suggestions during our fruitful discussions and for their valuable contributions to our work. The conversations with you were vital in inspiring me for the research. Thank you, Rafa, for hosting me at your institution in Madrid, and all the nice lunch conversations. I wish to thank Liliana Arrachea and Pablo Terren Alonso. I am grateful for getting the chance to collaborate with you, even from thousands of kilometers away. I would like to express my special thanks to Matteo Acciai, whose close collaboration made it possible to present our last paper in this thesis.

I am immensely grateful to Nastaran Dashti, who is as supportive a friend and as thoughtful a colleague I could hope for. Thank you for all the discussions, collaboration, and the nice time we spent together. You are among the most peculiar people I have ever met, and I hope to see a lot more of you. I wish you all the best for the next step of your journey.

I feel indebted to a great number of people that I can not name here. In particular, all previous and present members in Applied Quantum Physics group at MC2. It truly has been a very good time in this lab. Thank you for all the beautiful moments you made for me. My heartfelt thanks to my officemates for their kindness and patience. I thank my friends in quantum Device Physics and Quantum Technology groups for their company.

My time at Chalmers was made enjoyable in large part due to my Iranian friends here. I am grateful for the time spent with all of you. Thank you for

making Sweden feel like home. I thank Chalmers Karateklubb members and my sensei, Per Lundgren, for the great fighting time.

I would like to deeply thank my parents, sisters, Zahra and Leila, and my little brother Alireza, for their unwavering support and belief in me. Specially Leila for listening to my long speeches, and all your help. Last but not least, my partner Rui- you are a promise that I will never lose my smile, special thanks.

ABBREVIATIONS

BdG Bogoliubov-de Gennes.

COP coefficient of performance.

JJ Josephson junction.

Lor Lorentzian.

NS normal-metal-superconductor.

QD quantum dot.

QPC quantum point contact.

QSH quantum spin Hall.

RB rectangular barrier.

SNS superconductor-normal-metal-superconductor.

2-DEG two-dimensional electron gas.

LIST OF APPENDED PAPERS

This thesis is based on the work contained in the following papers:

- I.** F. Hajiloo, F. Hassler, and J. Splettstoesser “Mesoscopic effects in the heat conductance of superconducting-normal-superconducting and normal-superconducting junctions”,
Physical Review B **99**, 235422 (2019).
- II.** F. Hajiloo, P. T. Alonso, N. Dashti, L. Arrachea, and J. Splettstoesser “Detailed study of nonlinear cooling with two-terminal configurations of topological edge states”,
Physical Review B **102**, 155434 (2020).
- III.** F. Hajiloo, R. Sánchez, R. S. Whitney, and J. Splettstoesser “Quantifying nonequilibrium thermodynamic operations in a multiterminal mesoscopic system”,
Physical Review B **102**, 155405 (2020).
- IV.** M. Acciai, F. Hajiloo, F. Hassler, and J. Splettstoesser “Phase-coherent heat circulators with normal- or superconducting contacts”,
To be submitted (2020).

We always refer to these publications as Paper I, II, . . . , according to the labeling in the list above.

CONTENTS

Abstract	iii
Acknowledgements	v
Abbreviations	vii
List of appended papers	ix
Contents	xiii
1 Introduction	1
1.1 Thermoelectric cooling	2
1.2 Nonequilibrium effects	3
1.2.1 <i>Demonic</i> action of a nonequilibrium resource	3
1.3 Phase-coherent heat transport in normal- and superconducting devices	4
1.4 Thesis outline	6
2 Thermodynamic engines and operations	7
2.1 Controlling heat flow	7
2.1.1 Heat valve	8
2.1.2 Heat circulator	9
2.2 Heat engine	9
2.2.1 Steady-state heat engines using thermoelectrics	10
2.2.2 Power and efficiency	12
2.2.3 The second law and Carnot limit	12
2.3 Refrigerator	13
2.3.1 Thermoelectric and absorption refrigerators	13
2.3.2 Cooling power and coefficient of performance	14
2.3.3 The second law and Carnot limit	14
3 Nanodevices used for heat control	17
3.1 Two-dimensional electron gas (2-DEG)	18
3.1.1 Quantum point contact (QPC)	19
3.1.2 Quantum dot (QD)	20
3.1.3 Quantum Hall effect	22
3.2 Superconducting junctions	26
3.2.1 Bogoliubov-De Gennes equation	26
3.2.2 Josephson junction	27

4	Scattering theory	31
4.1	General background	31
4.2	Transport quantities	33
4.2.1	Charge and heat current operators	33
4.2.2	Linear response: charge and heat conductances	36
4.2.3	Charge and heat current noise	37
4.3	Superconducting systems	38
4.3.1	Scattering theory for superconductors	39
4.4	Transmission probabilities for specific devices	40
4.4.1	Transmission probability for a single level system with Lorentzian shape	40
4.4.2	Transmission probability for a rectangular barrier	41
4.4.3	Transmission probability for a quantum point contact	42
4.4.4	Transmission probability for a quantum spin Hall system	43
4.5	Scattering matrix for composed systems	45
4.5.1	Scattering matrix for an SNS junction	45
4.5.2	Scattering matrix for a complex system(ring structure)	47
5	Exploiting specific characteristics of mesoscopic devices to control heat	51
5.1	Thermoelectric cooling	51
5.1.1	Pendry's quantum bound	53
5.2	Nonequilibrium resource	55
5.3	Phase-dependent heat transport	56
6	Overview of the appended papers	59
6.1	Paper I	59
6.2	Paper II	60
6.3	Paper III	63
6.4	Paper IV	65
7	Summary	67
7.1	Outlook	69
	Appendices	71
	A Absorption refrigerator	73
	References	75
	Appended papers	87
	Paper I	89

Paper II	99
Paper III	119
Paper IV	141

1 Introduction

This thesis provides a study of thermal effects and heat transport in mesoscopic devices. A particular focus is on heat control exploiting unique effects occurring in systems confined to low dimensions and in systems operated in the quantum regime.

Mesoscopic devices have prospective applications in fields such as nanoelectronics and quantum technology. Their size lies between the atomic and macroscopic scales. In this regime, the system shows non-classical behavior. Such mesoscopic devices are often realized in nanometer-sized structures. In addition to the size, mesoscopic conductors need to operate at low temperatures in order to make quantum effects experimentally accessible [1]. The heating, along with the reduced thermal conductivity in thin layers of semiconductors such as silicon, due to quantum confinement effects [2], make major issues in the evacuation of the generated heat in nanodevices. This affects the functionality of these devices. To prevail over these harmful effects, heat currents dissipated in the systems need to be controlled and regulated to maintain the reliability of nanodevices.

Mesoscopic systems are also of fundamental interest since they exhibit quantum-mechanical properties due to their small sizes, and at the same time, it is possible to perform electronic transport measurements on them. Generally, electronic transport happens together with the transport of energy (since electrons carry both charge and energy), and part of this energy dissipates as heat.² Mesoscopic physics investigates how this electronic transport is influenced by quantum effects. The effects arising from size confinement and quantum features also influence the heat transport by electrons. This thesis, as the main subject of its study, investigates the exploitation of these effects to control heat.

Controlling and exploiting heat in mesoscopic systems is a topical field of interest [3–8] that would find applications in many fields of nanoscience, including thermal management, thermal isolation, energy harvesting, and cooling [9–12].

In addition to the practical interest in heat current control in nanodevices,

² Note that we do not treat heat transport due to phonons or photons, which in shielded low-temperature devices as the ones we consider, is suppressed.

there is a fundamental interest in heat transport in generic nanoscale structures. Recently, the field of *quantum thermodynamics*, the study of thermodynamical properties of quantum- and nanoscale systems, has gained much interest. In this context, for example, quantum heat engines and refrigerators have been theoretically studied [13–16]. Furthermore, the possibility of enhancing the efficiency of thermoelectric devices using quantum effects, for heat to electricity conversion and also energy harvesting [5, 17, 18], is currently addressed. Even in the classical regime, the thermodynamic behavior of small scale systems is fundamentally different from the one of macroscopic devices, which can typically be described by average, equilibrium properties. Nonequilibrium effects and fluctuations are the topics of the research fields of *nonequilibrium* and stochastic thermodynamics, see e.g. [19–22]. The theoretical results of this thesis contribute to these fields.

In this context, we consider various configurations of nanostructures and study heat transport in them. Our research has three main headings. On one hand, in paper II, we address thermoelectric cooling using energy filtering barriers. On the other hand, the thesis discusses the effects of nonequilibrium resources for heat-engine-type of systems that are the subject of paper III. Finally, we analyze the role of phase-coherent properties on heat flows that includes papers I and IV.

1.1 Thermoelectric cooling

To control heat, one can exploit thermoelectric properties of systems [23]. These properties relate electrical power to heat transport, making it possible to cool down a system using electrical power [3] or to produce electrical power (work) from heat.

Energy-filtering is at the basis of the thermoelectric performance of a system. This is done by a conductor that has an energy-dependent transmission, which can be due to quantum effects and size confinement. Famous examples of systems with energy-dependent transmissions are quantum point contacts (QPCs) and quantum dots (QDs). These systems have been investigated operating as quantum heat engines and refrigerators and they have shown large output power and efficiencies [23–25]. Among devices with energy-filtering characteristics, a novel system is a quantum spin Hall (QSH) device. In such a device, particles travel along counter propagating, spin-resolved edge channels called helical edge states. Recently, a QSH device in which the helical edge states are coupled through a magnetic island has been proposed as a thermoelectric [26]. Unlike quantum dot and QPC that have simple peak-shaped and step-like energy-dependent

transmissions, the QSH device shows complex features that we identified to be combinations of the ones in QPCs and QDs. The cooling power of this device had previously only been addressed in [26] for limited parameter regimes (linear regime). However, the thermoelectric cooling at large voltage and temperature differences (nonlinear regime) has not been considered. To illuminate this uncharted aspect, in paper II, we analyze the full cooling performance of the QSH device with a magnetic island. We also do a full performance analysis of the device, including the study of efficiencies, and present results for both linear and nonlinear regimes.

1.2 Nonequilibrium effects

Standard thermodynamics deals with equilibrium states. According to the zeroth law of thermodynamics, when two bodies are in thermal equilibrium with a third one, all of them have the same temperature. Nonetheless, microscopic systems can often not be well described by thermal equilibrium. Examples of these systems are not only the above described mesoscopic systems, but can also be found in biological and chemical systems. These systems have a nonequilibrium nature that can even stem from time-dependent or nonconservative forces. The field of stochastic thermodynamics describes these systems, addressing, for example, chemical reactions and biological processes from a thermodynamic perspective [27]. Namely, stochastic, nonequilibrium thermodynamics yields a description of microscopic systems, where fluctuations play an important role [28, 29].

In paper III, mesoscopic systems are investigated that are smaller than their thermalization length. This means, in particular, that particle distributions in the setup can not thermalize to equilibrium distributions. Most interestingly, it has recently been shown that nonequilibrium distributions can be used as a *resource*, instead or in addition to heat, which is standardly used as a resource for macroscopic thermodynamic engines.

1.2.1 *Demonic* action of a nonequilibrium resource

Using a nonequilibrium distribution as a resource, work can be done in some working substance without the need to inject any energy or heat into it, but by cooling down parts of the working substance [30, 31]. This reminds to some extent of a Maxwell demon, which can reduce the entropy of a gas of particles without doing any work on it.

Note, however, that there is a striking difference: A Maxwell demon relies on measurement and feedback on the microscopic degrees of freedom of the gas particles. The puzzle of the apparent contradiction with the laws of thermodynamics is solved when taking into account the heat dissipated when erasing the information acquired by the Maxwell demon from the measurements. Here, in the system of our interest, which is not information-driven, but operated by a nonequilibrium resource, the average work production in the working substance does not contradict the second law of thermodynamics for the following reason: entropy is produced in the nonequilibrium resource even in the absence of heat flow. This setup is therefore also referred to as an N-demon (where the "N" stands for nonequilibrium).

Following up on these initial studies [30, 31], it is of our interest to know more about the role of the nonequilibrium distribution. In paper III, we analyze the performance of devices acting similarly to a heat engine to produce power and to a refrigerator to perform cooling, but exploiting a nonequilibrium resource in addition to or instead of heat. For this, we specifically show how efficiencies of the machines can be used to identify the "demonic" action. Most importantly, we also propose a "free-energy efficiency", which fully captures the used resources.

1.3 Phase-coherent heat transport in normal- and superconducting devices

One class of particularly relevant nanoscale devices are setups containing superconducting elements, since also the heat transport in such junctions is remarkably influenced by the specific characteristics of superconductivity [3, 32]. One of these characteristics is the superconducting temperature-dependent energy gap. The energy gap makes superconductors good energy filters, in the sense that they only allow quasiparticles (constituting the energy carriers in superconductors) at specific energies to tunnel out from or into an electrode. Depending on the device operation, this makes the superconducting electrode or closely normal conductors to be cooled [33]. Therefore having superconducting elements as part of hybrid systems is useful for cooling: it allows for an implementation of electronic refrigerators [3], thereby improving the performance of electronic devices.

However, in this thesis, the focus is on superconducting junctions used as heat rectifiers and heat current switches [34, 35]. Here, another aspect of superconductors plays the most important role, namely the possibility of heat current control via the phase-dependence of superconducting junctions. It has been

theoretically predicted [32] that heat currents through so-called Josephson junctions, consisting of two superconductors separated by an insulator (SIS), depend on the relative phase of the superconducting condensates of the two superconducting regions. Only a few years ago, this intriguing effect was also proven experimentally [35, 36]. Since then, the study of phase-coherent caloritronics has caught a lot of attention in both theoretical and experimental researches, see [37] for a recent review.

These developments motivate theoretical studies on how phase-dependent heat transport depends on the properties of possibly complex hybrid (normal (N)- and superconducting (S)) junctions. The focus in this thesis is on junctions, consisting of extended, possibly diffusive, conductors, in which many transport channels with randomly distributed transmission probabilities can contribute to heat transport via quasiparticles. The impact of these transmission statistics on the phase-dependent thermal conductance has not received much attention so far.

In order to approach the role of complex junction properties on heat transport, we use a scattering matrix that allows us to straightforwardly implement different types of junction properties. We use this both for the theoretical description of the heat-conductance statistics of diffusive SNS junctions, but also for heat conductance calculations of NS junctions [38].

The possibility of controlling heat currents by the superconducting phase motivates the study of heat flows in other structures containing superconductors. In this work line, devices that have rarely been studied are heat circulators. These resemble circulators in electronics used, for instance, in radar or amplifier systems [39]. A heat circulator is a versatile device with two or more terminals, and when a heat current enters through one of the terminals, it will transmit in a particular direction. Recently, a three-terminal heat circulator with superconducting contacts has been suggested [40]. In this proposal, a three-terminal device composed of three superconducting contacts with a central scattering region and the presence of a magnetic field is suggested as a phase-coherent heat circulator. By changing the device's parameters, such as a magnetic field or superconducting phases, heat flows in a clockwise or anticlockwise direction. This type of device can be employed in phase-coherent caloritronics [37]. However, also in normal conducting systems, heat circulators would be of interest. In paper IV, we analyze the characteristics of a similar quantum heat circulator as proposed in Ref. [40] with an ideal ring shape structure for a setup composed of normal contacts and compare its performance with the superconducting one. Importantly, in paper IV, we study different types of circulators deviating from the ideal ring-shape circulator.

1.4 Thesis outline

The rest of this thesis is organized as follows.

Chapter 2 presents a brief overview of standard systems in thermodynamics that lead to heat control and exploiting heat for applications. Without aiming at a complete overview of the conventional thermodynamics, this chapter introduces the basic picture of thermodynamical systems required for following the research in this thesis. Chapter 3 introduces the relevant nanostructures considered in this thesis. Theoretical analysis of this thesis and appended papers are based on the scattering formalism. Chapter 4 formulates the transport quantities using this formalism and describes different types of scatterers introduced in chapter 3. These quantities are used to characterize and analyze the performance of systems studied in the appended papers. The focus of chapter 5 is the review of studies on the confinement and quantum effects we considered to exploit in order to control heat transport in the systems proposed in the appended papers. Chapter 6 gives an overview of the appended papers. In Chapter 7, the overall conclusions of the thesis are summarized.

2 Thermodynamic engines and operations

As mentioned in the previous chapter, developments in nanofabrication and mesoscopic devices motivate the investigation of controlling and exploiting heat flows using quantum properties [3]. Although thermodynamics have been started as a macroscopic theory more than a century ago, the laws of thermodynamics are persistent in quantum level to a large extent or can serve as a starting point for extensions. Therefore it is beneficial to review schemes and implementations of heat control at macroscopic scales.

In this chapter, some relevant example systems leading to the control and regulation of heat are briefly touched. In addition, the principles of performance of two major systems in thermodynamics, namely heat engines and refrigerators, and the laws limiting their performance are reviewed.

2.1 Controlling heat flow

Heat control and heat transfer are often alongside the fundamental concepts of thermodynamics. Heat transfer is the process of thermal energy transport through a material or from one body to another and usually transfers from hot to cold regions. This is well known from everyday life.

Controlling heat transfer is essential in a wide variety of fields in science and engineering. Controlling the direction and amount of heat flow is an essential matter, which is the subject of papers I and IV. In many fields, one of the goals of heat control is efficient energy consumption, for instance, in heating or cooling systems. An example of importance of temperature and heat control would be in electronics where they are crucial since heating in an electronic device affects its performance and can have harmful effects. Therefore, cooling of electronic components is a key matter in the industry. In this concern, paper II aims to reverse the flow of heat in order to perform cooling. Typically, systems which exploit heat use energy or heat flow as a resource. Apart from this, a resource other than (or in addition to heat) can be used to implement analogies to engines

and refrigerators. This is the topic addressed in paper III.

Controlling and exploiting heat in classical scales has a long tradition and is a known concept. This goes back to the beginning of industrial revolution and rise of thermodynamics [41]. Among relevant systems to exploit heat are heat engines, heat pump and refrigerators, heat valves, electronic heat sinks, heat circulators and so on. In the following, a number of these systems applicable for controlling and exploiting heat transfer are brought to attention.

2.1.1 Heat valve

Thermal valves or heat valves are a class of devices that are used to control heat in many applications and are known from daily life. Analogous to the electronic valves, heat valves control heat flows in electronic or thermal circuits. Among them are thermostatic radiator valves that are self-regulating devices that control an environment's temperature by changing the flow of hot water to the radiator, or thermostatic mixing valves that combine hot and cold water to ensure constant safe temperatures. There are also thermal expansion valves that are components in refrigerators and air conditioning systems that control refrigerant and heat flow in the system. In electronics, thermal valves can be useful in thermal management systems to limit the amount of heat flow in devices and remove waste heat from electronic components and batteries to prevent overheating. It is perceived from traditional applications that heat valves can be used to isolate and balance heat.

Due to particular relevance of control and manipulation of heat flow in mesoscopic systems [4], heat valves found their place in this field. In this regard, a number of proposals have been suggested. In particular, there was recently a proposed system that employs superconducting junctions as heat (thermal) valve [42]. In this work, phase-coherent property is used to control electronic heat conductance in Josephson junctions. This is related to paper I, where phase-coherent properties and temperature dependent energy gap in superconductors have been used for heat transport control and management in superconducting structures. A recent realization of a quantum heat valve that bridges mesoscopic thermodynamics to quantum information is in quantum systems composed of superconducting qubits [43]. These heat valves are relevant for the realization of quantum heat engines and refrigerators.

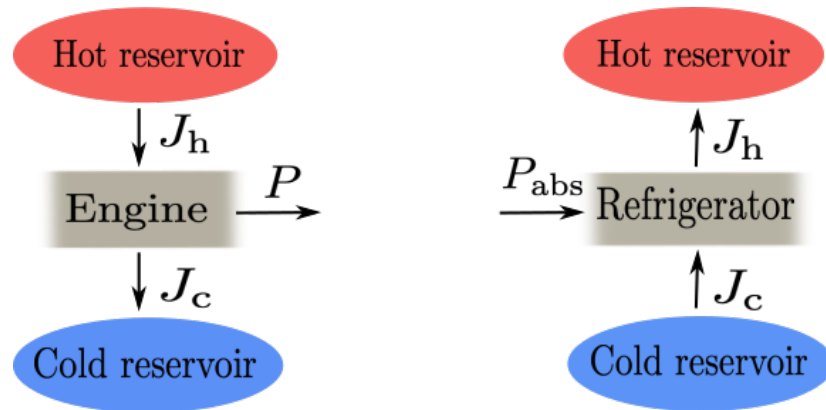


Figure 2.1: *Left: Heat engine. Part of the heat flow from the hot reservoir is converted to the output power in the working substance. Right: Refrigerator. Power is absorbed to cool down the cold reservoir.*

2.1.2 Heat circulator

Heat circulators are in analogy to charge current circulators that are widely used in electronics. A circulator in electronics is a non-reciprocal multi-port device that transports radio frequency or microwave signals in the clockwise or anti-clockwise rotational direction [44]. Breaking reciprocity and making one-way electronic components can help for example to enhance data capacity in wireless networks [45]. In a similar manner, heat circulators can be proposed. In thermal circuits, heat circulators can be used to route heat currents in thermal circuits and isolate them from unwanted parts of the device. Not only in thermal circuits, but heat circulators are also important tools in fields such as biology and chemistry, where sometimes there is a need to keep samples at specific temperatures. For this aim, typically a type of heat circulator called immersion circulator that uses a fluid for circulating heat are used.

At the nanoscale, there have been developments in achieving nonreciprocity using quantum effects [39, 46] and, recently, there have been efforts to establish that concept in thermal transport [40].

2.2 Heat engine

One of the means of exploiting heat is to use it for generating power in heat engines. Development of heat engines traces back to the beginning of thermodynamics [47] that started by the evolution of heat engines, and the principles behind the engines, that were evolved by Carnot [48] led to laws of thermodynamics. A heat engine is a system that converts heat or thermal energy into

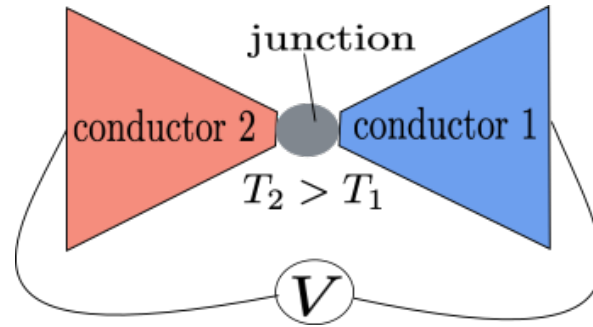


Figure 2.2: Sketch of a two-terminal system with two different conductors, and junctions at different temperatures, T_1 and T_2 and a voltage difference V .

mechanical or electrical energy or work [49]. This engine receives heat from a hot reservoir or a source with high temperature (T_h) and converts a portion of it to work. The remaining heat that is waste heat, is dumped to the surroundings or a cold reservoir with low temperature (T_c) as a sink. In Fig. (2.1) different components of a heat engine are schematically represented. There is a working substance that absorbs thermal energy (J_h) and generates work or power (P) out of it by exploiting its properties. The working substance can be fuel, gas, or a liquid.

2.2.1 Steady-state heat engines using thermoelectrics

A class of heat engines is based on the thermoelectric effect, which means that it transforms waste heat into electricity.

Consider two different macroscopic conductors connected in one end and, at the other ends, applied to terminals of a voltmeter, see Fig. (2.2). This system can be considered as a thermoelectric heat engine. One can apply a voltage bias or a temperature gradient or both to the two conductors. If there is only a voltage bias, it will result in a charge current flow. Besides, applying only a temperature gradient will make a flow of heat current. However, there exist other phenomena called thermoelectric effects. The first one was discovered in 1821 by T. J. Seebeck [50]. He showed that applying a temperature gradient to two conductors and heating the junction between them, without an electric field, will produce an electric current in addition to heat flow. This current is a thermoelectric current that in an open circuit results in a thermoelectric potential difference known as the Seebeck potential. J. Peltier observed the second of the thermoelectric effects in 1834 [51]. This effect tells us that if a charge current passes through two conductors' junction, depending on the direction of

this current, there will be a heating or cooling effect.¹ The Seebeck and Peltier effects are not independent. We see their dependence through coefficients that describe these two effects.

There has been recent interest in quantum systems as thermocouples, which are often referred to as three-terminal thermoelectrics [52]. Many works have pointed out how quantum mechanics can provide new approaches to design thermoelectric materials and devices [53, 54]. One of our interests in paper III is investigating possible thermoelectric effects in a suggested device configuration.

Onsager relations

Overall, applying voltage and temperature gradients will establish thermodynamic forces that impose charge (I) and heat currents (J). Assuming small voltage and temperature gradients, the thermodynamic forces are given by $F_e = \Delta V/T$ and $F_h = \Delta T/T^2$. Onsager relations give the relation of these forces to charge and heat currents as [55]

$$\begin{aligned} I &= L_{ee}F_e + L_{eh}F_h, \\ J &= L_{he}F_e + L_{hh}F_h, \end{aligned} \quad (2.1)$$

where the coefficients L_{ij} are Onsager coefficients. Using these coefficients one obtains the following transport coefficients: Electrical conductance, G , that is the ratio of charge current to the voltage gradient when no temperature gradient is present

$$G = \left(\frac{I}{\Delta V} \right)_{\Delta T=0} = \frac{L_{ee}}{T}. \quad (2.2)$$

Under the condition of zero charge current, the ratio of heat flow to the temperature gradient defines the thermal conductance, κ

$$\kappa = \left(\frac{J}{\Delta T} \right)_{I=0} = \frac{1}{T^2} \left(L_{hh} - \frac{L_{he}L_{eh}}{L_{ee}} \right). \quad (2.3)$$

Setting the charge current to zero, the Seebeck coefficient that is also called thermoelectric power in the literature [56], is obtained as

$$S = - \left(\frac{\Delta V}{\Delta T} \right)_{I=0} = \frac{1}{T} \frac{L_{eh}}{L_{ee}}. \quad (2.4)$$

¹ One should distinguish Peltier heating or cooling from Joule heating, which appears in conductors when a charge current flows in them and is related to the conductor's electrical resistivity.

The Peltier coefficient, indicated by M , is obtained by setting ΔT to zero

$$M = \left(\frac{J}{I} \right)_{\Delta T=0} = \frac{L_{he}}{L_{ee}}. \quad (2.5)$$

According to Onsager reciprocal relation in the absence of magnetic field, $L_{ij} = L_{ji}$, and therefore Seebeck and Peltier coefficients are dependent as $M = TS$. Besides this, the thermal and electrical conductances are related by the Wiedemann-Franz law that says the ratio of these two conductances is proportional to the temperature

$$\frac{\kappa}{G} = \frac{\pi^2}{3} \left(\frac{k_B}{e} \right)^2 T. \quad (2.6)$$

This ratio tells that the proportionality is the same for conductors at the same temperatures.

2.2.2 Power and efficiency

There are two most frequently used quantities that characterize the conversion of heat to work in heat engines. Those quantities are generated power and efficiency. Consider a heat engine that is an electrical system with two hot and cold reservoirs. In this system, the generated power in the working substance is

$$P = I\Delta V, \quad (2.7)$$

where I is the electrical current flowing against the voltage gradient ΔV . The typical definition of efficiency is the benefits extracted from the system with respect to the costs. Considering this definition for the efficiency of a heat engine gives a relation that is the ratio of the generated power to the input heat,

$$\eta = \frac{P}{J_h}, \quad (2.8)$$

with J_h referring to the heat flowing out of the hot reservoir into the working substance.

2.2.3 The second law and Carnot limit

The operation of heat engines is bounded by limits imposed by the second law of thermodynamics [57]. The second law originates from the fact that heat naturally flows from hotter to colder bodies. The second law in heat engines can be formulated as the statement that the complete conversion of heat into work is impossible (Kelvin's statement). This statement rules out the perfect engine.

The Carnot efficiency is a manifestation of the second law in heat engines, and it is universally valid. Carnot's theorem provides the upper bound on a heat engine's efficiency working between two reservoirs at temperatures T_h and T_c . This theorem tells us that this heat engine can not be more efficient than a Carnot engine operating between the same hot and cold temperatures. Carnot engine is a reversible engine operating between a source at temperature and a sink at temperatures T_h and T_c , respectively. The efficiency of the Carnot engine is

$$\eta^{\text{Carnot}} = 1 - \frac{T_c}{T_h}. \quad (2.9)$$

This sets a maximum limit to heat engine efficiencies that depends only on the two temperatures [52].

In the quantum regime, when the baths are thermal, the Carnot efficiency limit is equally applicable for a small quantum system. However, if the baths are nonthermal, the story changes. We address the changes in the limits of efficiencies in paper III.

2.3 Refrigerator

2.3.1 Thermoelectric and absorption refrigerators

As the natural flow of heat is from regions with high temperatures to low temperature ones, the reverse process can be done by refrigerators. Refrigeration has a high impact in everyday life and industry, and the high demand for cooling in many fields provided the practical impetus for developments of the science of refrigeration.

One type of common refrigerators that can be called thermoelectric refrigerator is like a heat engine running backward, that is it absorbs work or power (P_{abs}) to extract heat from a cold reservoir (J_c) and dumps out this heat into a hot reservoir (J_h), depicted in Fig. (2.1). Here cooling is done by electrical power.

Another type of refrigerator that is called absorption refrigerator performs cooling by heating. In these types of systems, heat is directly used to do cooling. This gives another evidence for waste heat to be useful. In cooling by heating, a heat source that can be waste heat is used as a source to provide energy to drive the cooling process. Traditionally these refrigerators are used when electricity is not available. An absorption refrigerator has three reservoirs, two in high (T_h) and low (T_c) temperatures and one at ambient temperature (T_0). The heat flow from the hot reservoir to a reservoir at T_0 is used to drag

heat out of the cold reservoir [52].

The study of cooling by heating has also become popular in quantum systems [33, 58, 59]. In paper III we address the performance of an analogy to an absorption refrigerator in a device operated by a nonequilibrium resource.

2.3.2 Cooling power and coefficient of performance

Analogous to a heat engine, refrigerators' performance is characterized by two quantities that are cooling power and coefficient of performance or COP. Cooling power is defined as the heat current J_c that flows out of the cold reservoir. The COP of a standard refrigerator that is in principle the efficiency is defined as the ratio of cooling power that is the outcome of refrigeration, to the absorbed power that is the cost,

$$\text{COP} = \frac{J_c}{P_{\text{abs}}}. \quad (2.10)$$

If the absorbed power is electrical power, it will be equal to $P_{\text{abs}} = -I\Delta V$. In absorption refrigerators, the efficiency is defined as the ratio of the cooling power that is the benefit, to the cost that is the heat flow out of the hot reservoir (that is driving the process),

$$\text{COP}_{\text{abs}} = \frac{J_c}{J_h}. \quad (2.11)$$

2.3.3 The second law and Carnot limit

Considering the second law for refrigerators, one can make the statement that there is no refrigerator that can transfer heat from a colder to a hotter reservoir without using any work or power (Clausius's statement).

The performance of a refrigerator is bounded by the Carnot coefficient of performance that is the maximum efficiency a refrigerator can get when it is operating between a cold and hot reservoir with temperatures T_c and T_h and is given by

$$\text{COP}^{\text{Carnot}} = \frac{T_c}{T_h - T_c}. \quad (2.12)$$

It is worth to note that the laws of thermodynamics let the coefficient of performance to exceed one [52].

For absorption refrigerator the upper bound on efficiency is given by

$$\text{COP}_{\text{abs}}^{\text{Carnot}} = \frac{1 - T_0/T_h}{T_0/T_c - 1}, \quad (2.13)$$

where T_0 is the environment temperature. This efficiency is the same as the Carnot heat engine's efficiency, whose power output goes into a Carnot refrigerator [52].

3 Nanodevices used for heat control

We have already underlined the importance of heat transport control in mesoscale. Mesoscopic devices belong to a category of systems in nanometer size. These devices are particularly relevant in quantum technologies. In this regards, nanostructures such as two-dimensional electron systems, quantum dots, and superconducting structures are widely employed [60–64]. This makes it important to gain a broader insight of capabilities and characteristics of these structures. The study of fundamental principles behind the operation of nanodevices are accessed in mesoscopic physics. One of the aims of this field is to understand nanoscale systems and devices. It investigates the quantum mechanical properties of particles such as electrons. In this spirit, in the arena of mesoscopic physics, building devices in which there is control over transport of carriers are crucial. Confinement of electrons in nanostructures led to development of one type of these systems that is two-dimensional electron gas (2-DEG). Among confined systems, quantum dots caught attention since they can be integrated with both electronic and photonic components in miniaturized chips. Quantum dots are one of the structures that made it possible to control charge flux down to the single particle level [65].

This chapter introduces a few nanostructures essentially relevant for this thesis. Parts of the devices we focus on are confined systems at the nanoscale including quantum Hall structures, quantum point contacts, and quantum dots. Here, we summarize some of the features of these systems. To do so, this chapter begins with a review over two dimensional electron gas (2-DEG) and formation of quantum point contacts (QPCs) and quantum dots (QDs) out of a 2-DEG. The chapter then provides an introduction on the quantum spin Hall (QSH) device.

Another class of highly relevant devices that we study in papers I and IV contain superconducting junctions. Description of some relevant properties of these junctions are presented in the second part of this chapter.

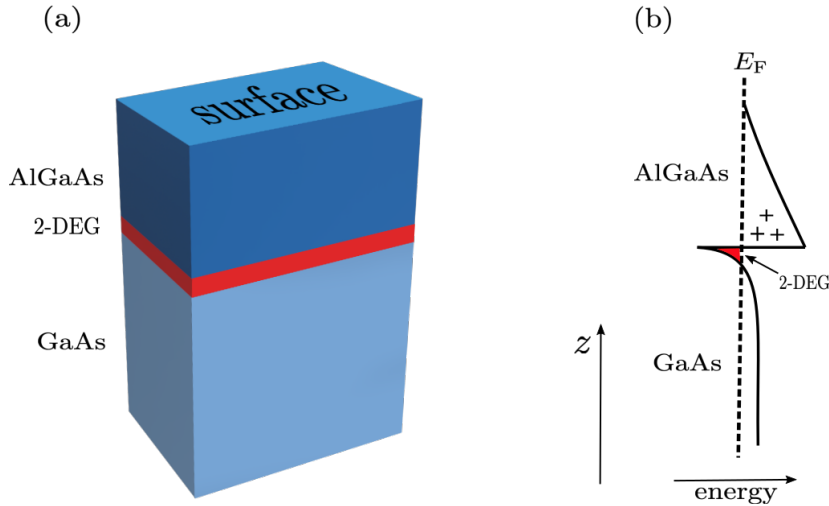


Figure 3.1: (a) Layers of a GaAs/AlGaAs heterostructure. (b) Conduction band of a junction of n-type AlGaAs and GaAs. A 2-DEG forms at the interface.

3.1 Two-dimensional electron gas (2-DEG)

The two-dimensional electron gas or 2-DEG has been extensively used in the study of transport properties in mesoscopic systems. It is a system of electrons confined in one dimension. A common 2-DEG can be found in metal-oxide-semiconductor (MOS) structures, for instance in the interface of silicon oxide (SiO_2) and p-doped silicon (p-Si) [66]. In this case, the 2-DEG gets formed at the semiconductor-insulator interface. One can also form a 2-DEG as a conducting interface between two different semiconductors. A material system that provides a high-quality conduction channel is a heterojunction of gallium arsenide (GaAs) and aluminum gallium arsenide (AlGaAs) [67]. Growing a GaAs substrate and on top of that, AlGaAs, a thin two-dimensional conducting layer forms in the interface.

GaAs has a smaller bandgap than AlGaAs. When an n-doped AlGaAs (silicon donors can be used) is in contact with GaAs, the Fermi energy in the wide gap side is higher than the narrow gap. This results in electrons flowing away from n-AlGaAs, leaving positively charged dopants behind. What happens then is that due to this charge and the resulting electrostatic potential, there is a peculiar band bending effect in the conduction band next to the interface that forms a triangular-shaped confinement region, see Fig. (3.1). This creates a potential well with bound states in it. In this region, the Fermi level is inside the conduction band. The sharp peak of electron density in the interface corresponds to a 2D free electron gas constrained in one dimension. In a typical structure, the 2-DEG is buried in about 100 nm below surface of the crystal, and it is not on

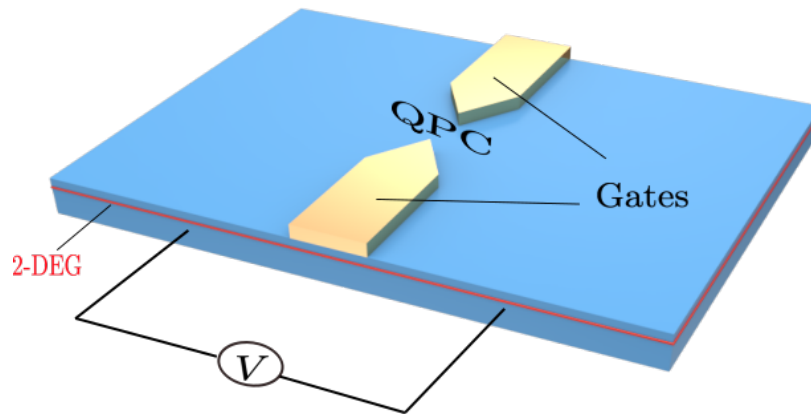


Figure 3.2: Schematic representation of QPC. Two metal gates (golden) deposited on top of a 2-DEG make a constriction (QPC) by depleting the region below the gates from electrons. The voltage bias V drives electrons through QPC.

the surface.

The two dimensional electron gas is the basic system to form structures with more confinement on electrons, such as quantum point contact (QPC) and quantum dots. Moreover, the quantum Hall effect was first observed in 2-DEG [68]. In papers II and III, the electron transport in QPC, quantum dots, and through edge states in a quantum Hall system is considered.

3.1.1 Quantum point contact (QPC)

Confining electrons further, brings them from two to one dimension where quantum point contact arises. This section explains how the quantum point contact (QPC) is made out of a 2-DEG. QPCs are constrictions created by gate voltages in different nanoscale conductors such as a 2DEG. They are shaped electrostatically with the gate electrodes [69–71]. Gates are metals placed on top of a crystal. Consider a system of 2-DEG, as depicted in Fig. (3.2), with two gates placed on top connected capacitively to the 2DEG, with a gap between the gates (split-gate configuration). When applying a negative voltage on the golden gates, this potential will repel electrons from underneath the gates and induce a positive charge in the 2-DEG. If the gate is continuous and goes all the way across the 2-DEG without splitting, for a very negative potential on the gate, the 2-DEG will be separated in two disconnected parts with a region depleted of electrons in between. For the split gates configuration, depleting the region underneath the gates will produce imprints of the gates in the 2-DEG, where there will be no electrons. This makes a constriction where the number of channels of 2-DEG remained is comparable to electron's wavelength. This structure is called a quantum point contact and is a remarkable example of a

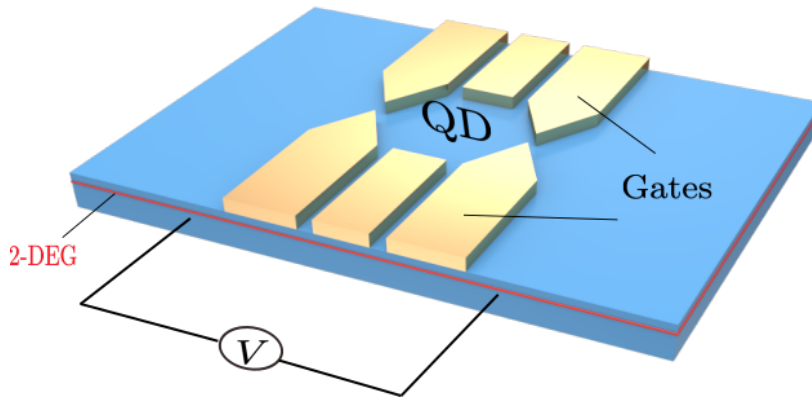


Figure 3.3: Schematic representation of a quantum dot configuration in a 2-DEG. The Golden area represents the metal gates, similar to the QPC structure. The central region is the dot connected by QPCs to the rest of the 2-DEG region [75].

one-dimensional system. This system is fully controllable, and one can change its width and length by gate configuration. The quantization of charge conductance in QPCs is a well-known property that was experimentally observed in 1988 [72]. Shortly after that, experiment on thermopower measurements in QPC was reported [73].

From particles arriving at QPC only a finite number of them are transmitted. These are distinguished as open and closed channels [74]. The probability of this transmission that is dependent to energy of particles, is describes in chapter 4.

3.1.2 Quantum dot (QD)

A full confinement of electrons leads to formation of quantum dots. In a 2-DEG system, using patterned electrostatic gates, one can make different kinds of constrictions. One example is QPC that is explained in the last section. Now consider another structure called quantum dot observed in an experiment in 1988 in a 2-DEG in the interface of GaAs/AlGaAs [76, 77]. Similar to QPC, using metallic gates to deplete the regions below the gates in 2-DEG can make zero-dimensional islands, see Fig. (3.3). These islands are charged islands with the size of the order of electron's wavelength and are famous as quantum dots (QDs). This type of constriction is confined in all three directions, and because of this, a QD is sometimes referred to as a zero-dimensional system [78].

The shape and size of the dot can be controlled by gate voltages. The small size of the island says that electrons are confined to discrete levels. In the QD configurations, a quantized number of electrons, ne , can locate with n being an

integer number. The transport properties of a QD can be measured by coupling it to leads and passing current through the dot.

QDs are of interest for thermoelectric applications and their thermoelectric properties have been investigated both in theory and experiment [79–81]. The focus on quantum dots in this thesis is their use in the transport of charge and energy (heat). We consider single level Lorentzian quantum dots. This is employed in papers II and III in the devices we study.

An electron that tunnels onto the island has to overcome a certain Coulomb potential, which can be large due to small capacitance resulting from the small size of the quantum dot. When charges are confined in three dimensions, one needs to consider the capacitance effect since capacitance becomes very small, and that means the charging energy becomes large. The energy required to add one electron to a QD with n number of electrons on the QD is determined by the charging energy due to the Coulomb potential [82]. Charging energy for one electron is $E_c = e^2/C$ where C is the capacitance. The charging energy for an island with the size 100 nm is of the order of 1 meV. If $k_{BT} \gg E_c$, the charging energy can be neglected [78].

Aharonov-Bohm ring

Aharonov-Bohm (AB) effect is about quantum mechanical effects that arise when a particle passes through a region with nonzero vector potential. An experimental arrangement that was suggested in a 1959 paper by Aharonov and Bohm tells that a charged particle confined to a circular ring in a region with a nonzero vector potential (\mathbf{A}) is affected by the presence of \mathbf{A} .

The applicability of quantum dots for exploring phase-coherent properties in mesoscopic physics [83] led to realization of AB rings using quantum dots [84]. This has been investigated in numerous studies to fabricate high quality quantum rings [85] and to assess Aharonov-Bohm features with QD in one or two arms of the interferometer or a triple quantum dot configuration [86–89]. It has also been demonstrated in a recent experiment that interferometry can be used to readout a QD defined in a nanowire that is useful in the interferometric readout of qubits [90].

A ring structure configuration composed of quantum dots is considered in this thesis in the structure of a heat circulator considered in paper IV.

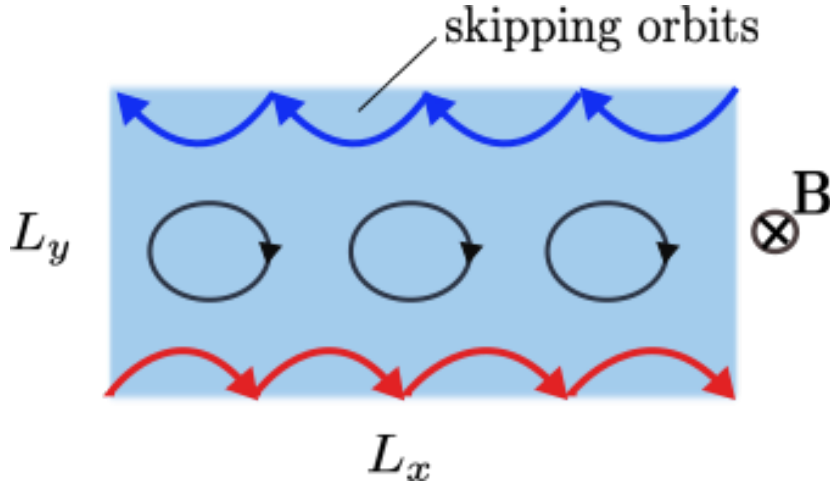


Figure 3.4: Schematic illustration showing right and left moving skipping orbits of particles at edges of the sample in a perpendicular magnetic field.

3.1.3 Quantum Hall effect

The classical Hall effect was discovered in 1880 [91], and it is explained as the following. Consider a two dimensional plane of a conductor, to which a perpendicular magnetic field is applied. Pushing current through the plane in the x -direction, as shown in Fig. (3.4), it is observed that in addition to the usual longitudinal voltage that exists for any accessive conductor, one can also measure a transverse voltage, V_H , (Hall voltage) across the sample. What is happening is that as charge q , carried by the current in x -direction, enters the magnetic field region, its trajectories curve due to the Lorentz force. Therefore opposite charges accumulate at the two edges of the sample in y -direction, which means an electric field is set up in the y -direction. What is measured in experiment is the Hall resistance, $R_{xy} = V_H/I$, where I is the current density, j_x times L_y . One finds $R_{xy} = B/qn$, n being an integer, that shows R_{xy} is linearly dependent to B with the slope being the density of charge carriers. By cooling the sample one starts to see the appearance of steps instead of the straight line, and when the temperature is low enough, the steps get very sharp and form plateaus. The value of the Hall resistance at the plateaus is found to be h/ne^2 , where n is an integer [92]. This is the phenomenon of (integer) quantum Hall (QH) effect.

Edge states in quantum Hall

Consider an electron close to the edge of the sample. This particle moving in a curved trajectory might run into the edge, then it will scatter and bounce off the edge under the influence of Lorentz force, and it will travel along the edge in a skipping orbit trajectory, see Fig. (3.4). This is the classical view. Quantum

mechanically, the wave function of the electrons are confined in one-dimensional edge channels. In this effect, backscattering of electrons is impossible. Therefore this channel is not only simply one-dimensional, but it is a channel where particles can only move one way since the magnetic field forces particles to move only in one dimension. These channels are known as chiral edge channels. We here show a simple description of edge state transport that can explain the plateaus in the Hall resistance.

Consider a noninteracting two dimensional system of electrons (2-DEG) with dimensions L_x and L_y . The electrons in this system with charge e and effective mass m^* under an applied perpendicular magnetic field, have the Hamiltonian $H = (\mathbf{p} - e\mathbf{A})^2/(2m^*)$ with \mathbf{A} being the vector potential resulting from the magnetic field. Taking the magnetic field in the z -direction, the vector potential in Landau gauge can be written as $\mathbf{A} = -By\hat{e}_x$. The y component of momentum, p_x commutes with the Hamiltonian, $[p_x, H] = 0$, therefore the eigenstates of p_x are plane waves in x direction. To solve the Schrödinger equation we make an ansatz

$$\psi(x, y) = e^{ikx}\phi(y), \quad (3.1)$$

where k is the momentum in x -direction. Choosing periodic boundary condition gives $e^{ik(x+L_x)} = e^{ikx}$. This tells us $kL_x = 2\pi j$ with an integer j . Now we consider the Schrödinger equation to solve it for $\phi(y)$. Here we consider a confinement potential, $V(y)$

$$\frac{1}{2m^*} \left[-\hbar^2 \frac{\partial^2}{\partial y^2} + (-i\hbar\partial_x + eBy)^2 + V(y) \right] e^{ikx}\phi_k(y) = Ee^{ikx}\phi_k(y). \quad (3.2)$$

Taking a parabolic confinement potential $V(y) = m^*\omega_0^2 y^2/2$ as suggested in [93] and substituting this into Eq. (3.2) we obtain

$$\left[-\frac{\hbar^2}{2m^*} \frac{d^2}{dy^2} + \frac{1}{2}m^*\omega^2(y - y'_0)^2 + \frac{1}{2}m^*\frac{\omega_c^2\omega_0^2}{\omega^2}y_0^2 \right] \phi_k(y) = E\phi_k(y), \quad (3.3)$$

where the guiding center is $y_0 = l^2k$ and $l = \sqrt{\hbar/eB}$ is the magnetic length. The Eq. (3.3) shows a harmonic oscillator with the center at $y'_0 = y_0\omega_{c^2}/\omega^2$ where $\omega^2 = \omega_{c^2} + \omega_0^2$ and $y_0 = -l^2k$. $\omega_c = eB/m^*$ is the cyclotron frequency. Using the definitions of y_0 and the magnetic length we have $k = m^*y_0\omega_c/\hbar$ and then we can write the last term on the left side of Eq. (3.3) as

$$\frac{1}{2}m^*\frac{\omega_c^2\omega_0^2}{\omega^2}y_0^2 = \frac{\hbar^2k^2}{2M}, \quad (3.4)$$

where $M = m^*\frac{\omega^2}{\omega_0^2}$. Finally the eigenenergies of the harmonic oscillator in Eq. (3.3) are

$$E_n = \left(n + \frac{1}{2} \right) \hbar\omega_c + \frac{\hbar^2k^2}{2M}. \quad (3.5)$$

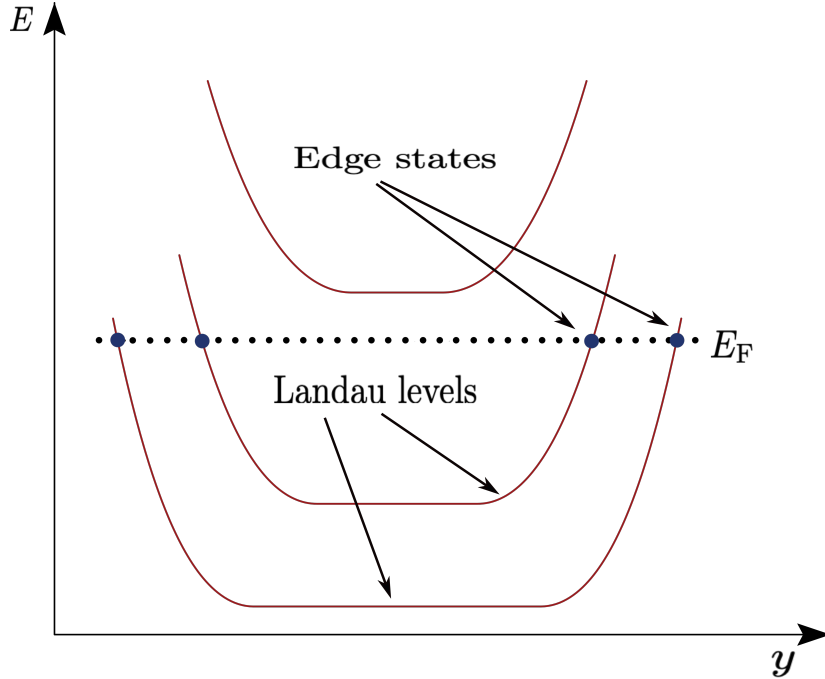


Figure 3.5: Landau-level energies at the bulk and edges of a quantum Hall sample.

We see that in the case of no confinement, the energy levels are degenerate. These eigenenergies correspond to transport channels in the scattering picture. These Landau-level energies are shown in Fig. (3.5). The bulk Landau levels are filled and separated from the Fermi level and hence do not participate in conduction, resulting in zero currents in the bulk of the sample. Near the edge, the Landau levels rise and cross the Fermi level. Therefore, for one filled bulk Landau level, there are only two Fermi points, a right and left moving ones, confined to the top and bottom edge of the sample, and contribute to creating a current flow at the edges. As a result, the bulk remains insulating, and there are chiral edge channels where the particles propagate in two different directions, which gives rise to the Hall conductance.

Quantum spin Hall (QSH)

In contrast to the quantum Hall effect that exists only in the presence of magnetic fields, a so-called quantum spin Hall effect that was theoretically predicted in 2006 [94] and experimentally realized in 2007 in HgTe quantum wells [94] happens in the absence of any magnetic field .

In the spin Hall (SH) effect, a spin current flows in a transverse direction in response to an applied electric field in a longitudinal direction. Unlike the Hall effect, which happens in the presence of an applied magnetic field, the SH effect does not need any magnetic field. What leads to the intrinsic spin Hall effect is

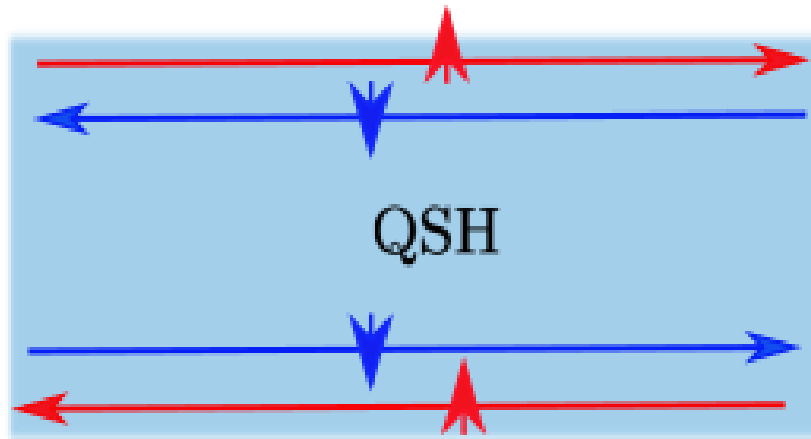


Figure 3.6: Helical edge states in quantum spin Hall (QSH) effect. The top edge has a right-mover channel with spin up (red) and a left-mover with spin down (blue), and conversely for the lower edge.

the spin-orbit interaction.

Quantized spin Hall effect can be understood as two copies of the integer quantum Hall states, one for up and one for down spins. The two spins in one edge flow in opposite directions in the presence of an electric field, Fig. (3.6) therefore there is no net Hall current, but there is a net flow of spin. This spin current defines a quantized spin Hall conductivity, which refers to the name quantum spin Hall (QSH) effect. The edge states for up and down spins propagate in opposite directions. These are called helical edge states. The results of computing the eigenstates using tight-binding model show a bulk energy gap between valence and conduction bands, but inside this gap, some bands are localized at the edge. The up and down spins have positive and negative group velocities respectively.

To backscatter at the same edge, an electron requires a spin-flip on edge, which requires the breaking of time-reversal symmetry. Since time-reversal symmetry is preserved, no backscattering is allowed. While the presence of a magnetic field and breaking of time-reversal symmetry induces backscattering along with the edge states, it has been shown that inter boundary scattering is possible at a constriction like a QPC in the absence of a magnetic field [95]. In this work, spin preserving tunneling between the opposite edges is investigated in a Fabry-Perot interferometer. In another work, a tunnel junction between helical edge states has been studied via a constriction in a QSH system [96]. In this work, a constriction is considered in a four-terminal quantum spin Hall setup that induces an electron-tunnel coupling between the helical edge states in the two opposite edges.

3.2 Superconducting junctions

Superconducting devices are well paired up with nanotechnology due to their versatile and notable characteristics. One of the specific interests of this thesis is devices containing superconducting junctions, namely hybrid structures of normal-metal and superconductors. In order to formulate the scattering formalism in superconductors in the next chapter, we first here explain some basics of the behavior of superconducting transport states.

3.2.1 Bogoliubov-De Gennes equation

The Bogoliubov-De Gennes equation (BdG equation) describes the behavior of superconducting states. The scattering states in superconductors are eigenfunctions of the BdG equation that has the form of two Schrödinger equations for electron and hole wave functions coupled via the superconducting energy gap.

$$i\hbar \frac{\partial f}{\partial t} = \left[-\frac{\hbar^2 \nabla^2}{2m} - \mu(x) + V(x) \right] f(x, t) + \Delta(x)g(x, t), \quad (3.6a)$$

$$i\hbar \frac{\partial g}{\partial t} = - \left[-\frac{\hbar^2 \nabla^2}{2m} - \mu(x) + V(x) \right] g(x, t) + \Delta(x)f(x, t). \quad (3.6b)$$

Here $\Delta(x)$ is the space dependent energy gap and $\mu(x)$ is the chemical potential. In a normal metal [that is, for $\Delta(x) = 0$], Eqs. (3.6) are two independent Schrödinger equations for electrons and holes. On the contrary, in a superconductor we have $\Delta(x) \neq 0$, and the electron and hole wave functions are coupled. We now assume that $\mu(x)$, $\Delta(x)$ and $V(x)$ are all constant. As a result, the solutions for Eqs. (3.6) are plane waves $f = ue^{ikx - iEt/\hbar}$ and $g = ve^{ikx - iEt/\hbar}$. The amplitude $|v|^2$ represents the probability that a pair of states (\mathbf{k} , $-\mathbf{k}$) is occupied, whereas $|u|^2$ is the probability that such a pair of states is unoccupied, which also implies $|u|^2 + |v|^2 = 1$. In the absence of an external field $V = 0$, substituting f and g into (3.6) gives:

$$Eu = \left(\frac{\hbar^2 k^2}{2m} - \mu \right) u + \Delta v, \quad (3.7a)$$

$$Ev = - \left(\frac{\hbar^2 k^2}{2m} - \mu \right) v + \Delta u. \quad (3.7b)$$

Now, we want to obtain the dispersion relation for a superconductor. To do this, we need to calculate u or v by solving the set of equations (3.7). Eventually, this procedure allows for finding the Bogoliubov spectrum (dispersion relation)

$$E^2 = \left(\frac{\hbar^2 k^2}{2m} - \mu \right)^2 + \Delta^2, \quad (3.8)$$

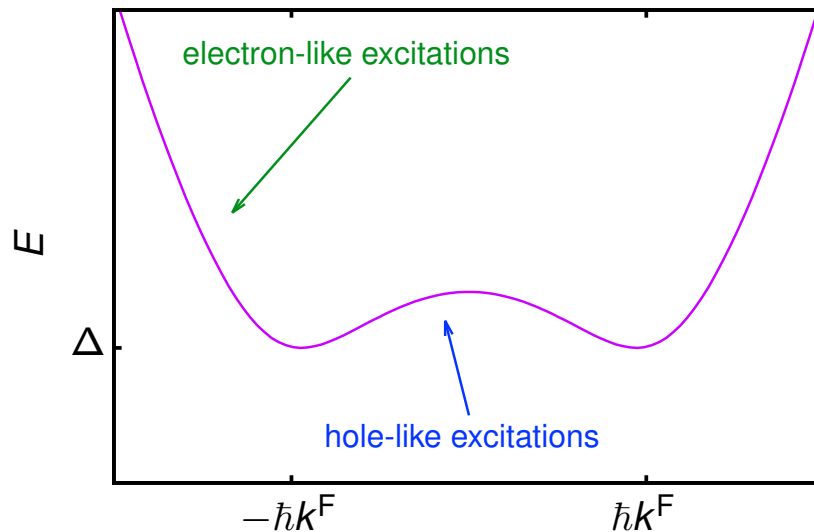


Figure 3.7: Dispersion relation for a superconductor, see Eq. (3.8), showing the energy gap of a superconductor.

which is also illustrated in Fig. (3.7). Solving the equation above for the wave vector, we get

$$\hbar k^{\pm} = \sqrt{2m(\mu \pm \sqrt{E^2 - \Delta^2})}. \quad (3.9)$$

The two momenta k^+ and k^- correspond to particle- (electron-) and hole-like excitations, respectively. Knowing that $|u|^2 + |v|^2 = 1$, we have the energy dependences of u and v

$$|u|^2 = \frac{1}{2} \left(1 \pm \frac{(E^2 - \Delta^2)^{1/2}}{E} \right) = 1 - |v|^2. \quad (3.10)$$

The Bogoliubov spectrum illustrated in Fig. (3.7) corresponds to the spectrum of quasiparticles in superconductors and there is a gap in the energy spectrum. This energy gap indicated by Δ , is considered as a temperature and phase dependent gap $\Delta = |\Delta(T)|e^{i\varphi}$ [97].

The Bogoliubov states are used to calculate the scattering (reflection and transmission) amplitudes in order to obtain the transport quantities in superconducting junctions from scattering theory in chapter 4.

3.2.2 Josephson junction

One of the hybrid structures we concentrate on is the Josephson junction—a structure containing two superconductors connected by an insulator (SIS) or

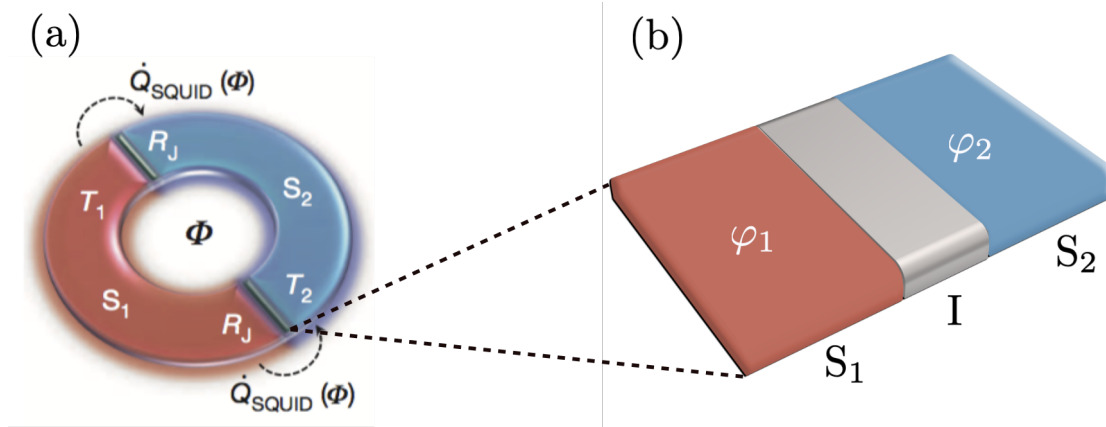


Figure 3.8: (a) Scheme of a temperature biased SQUID made of two identical superconductors S_1 and S_2 . R_J is the normal state resistance of each junction and $\dot{Q}_{\text{SQUID}}(\Phi)$ is the heat current flowing from the hotter to the colder superconductor [36]. (b) Structure of a Josephson junction with two superconductors with different phases φ_1, φ_2 ($\Phi = \varphi_1 - \varphi_2$).

a small normal metal conductor (SNS), Fig. (3.8). Indeed, Josephson junctions form the basis of an extensively used device, the superconducting quantum interference device (SQUID) [98]. In panels (a) and (b) of Fig. (3.8) a scheme of this device and a Josephson junction respectively, are shown. Transport across Josephson junctions is governed by the phase difference between the two superconducting condensates of the junction. This phase difference leads to a *dissipationless* charge current in the absence of any bias voltage. This current is a supercurrent that can flow between two superconductors across a non-superconducting material. This charge current is carried by Cooper pairs, and depends on the phase difference of the two superconducting condensates (Φ) through the relation $I_s = I_c \sin \Phi$ where I_c is the critical current that is the maximum supercurrent that can flow. To explain this, we can think of evanescent tails of the two superconductors' wave functions in the barrier between the two superconductors. When the two superconductors are close enough (for a barrier thickness shorter than the superconductor's coherence length), these tails overlap, which makes the transport of cooper pairs happen [97]. This famous effect is known as the Josephson effect and has first been predicted by Brian Josephson [99, 100]. Importantly, this current flows in the absence of any heat current!

However, when a temperature bias is applied between the two superconductors, there will be a heat current flowing through the junction. This heat is carried by electron- and hole-like quasiparticle excitations in the superconductors at energies above the superconducting gap. This heat current's striking property is its dependence on the phase difference of the two superconducting

condensates, as predicted by Maki and Griffin [32] and illustrated by [36]. We study this phase-dependent heat transport using the scattering theory formalism in paper I.

As we see in the formulation of heat current in chapter 4, the phase dependency of heat current is through the transmission probability of the Josephson junction. This phase-dependent transport of quasiparticles across the junction takes place via Andreev reflection at the superconductor's interface. The Andreev reflection is a type of particle scattering that occurs at the interfaces between a superconductor and a normal conductor and consists in a back reflection of, e.g., an electron-like quasiparticle into a hole by transferring a charge of $2e$ to the superconductor [101]. For the heat current considered in paper I, also Andreev reflection *above* the gap is relevant.

4 Scattering theory

The theoretical approach we use to study electronic charge and heat transport is scattering theory. The scattering theory of electronic transport in mesoscopic conductors, as we use it here, was first developed by Landauer and Büttiker, see Refs. [102–105] for seminal papers and [106] for reviews. The scattering theory gives intuitive, simple descriptions about transport phenomena, and it is most applicable for systems in which the many-body interaction between particles is negligibly small. In this chapter, we review the properties of the scattering theory for normal and superconducting systems. We then introduce different probabilities for nanostructures, which are considered in the appended papers.

4.1 General background

Electrons undergo scattering while traversing nanostructures. These scatterings which affect the transport properties can be due to defects in nanostructures or potential barriers. A scattering matrix describes this scattering. Let us assume a multi-terminal nanostructure consisting of a central scattering region connected to reservoirs via perfect leads, as presented in Fig. (4.1). All the reservoirs are at thermal equilibrium with different temperatures T_α and chemical potentials μ_α . A particle flux coming into the scatterer from one of the reservoirs is scattered in the central region. These particles are either reflected or transmitted to any of the other reservoirs. The wave functions of particles emitted from a reservoir can be written as a linear combination of plane waves [74]

$$\psi(\mathbf{r}_\alpha) = \sum_n^{\mathcal{N}} \frac{1}{\sqrt{2\pi\hbar v_{\alpha n}}} \Phi_{\alpha n}(y_\alpha, z_\alpha) [a_{\alpha n}(E) e^{ik_x^{(\alpha n)} x_\alpha} + b_{\alpha n}(E) e^{-ik_x^{(\alpha n)} x_\alpha}]. \quad (4.1)$$

Here, the indices α and n respectively indicate different leads and transport channels and \mathcal{N} denotes the total number of channels. Particle velocity in channel n is indicated by $v_{\alpha n}$ and $\Phi_{\alpha n}$ is the transverse wave function. The wavefunctions propagate along the axis x_α and $\mathbf{r}_\alpha = (x_\alpha, y_\alpha, z_\alpha)$ with y_α and z_α being the transversal directions. The wave vector depends on energy as $k_x^{\alpha n} = \sqrt{2m(E - E_{\alpha n})/\hbar}$ with $E_{\alpha n}$ representing the energy of particle with mode n in lead α . We here assume that particle scattering happens without energy loss; in other words, it is elastic. The coefficients $a_{\alpha n}$ and $b_{\alpha n}$ are respectively

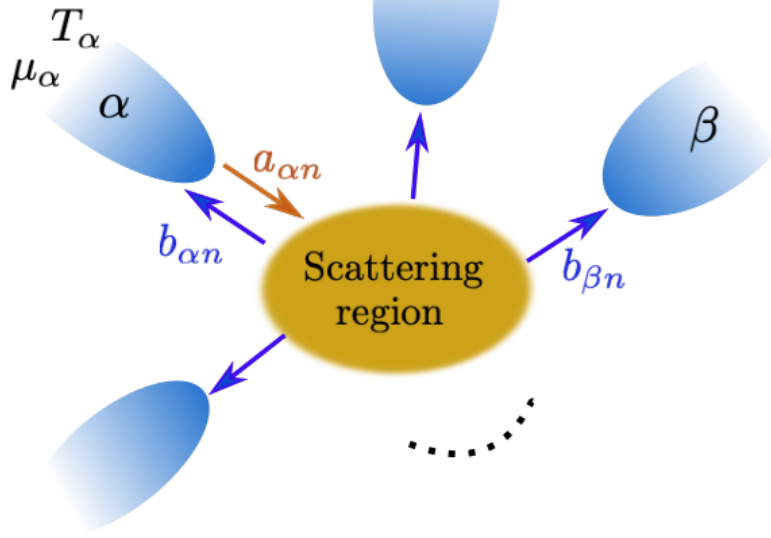


Figure 4.1: schematic representation of a multi terminal mesoscopic conductor with a central scattering region.

the amplitudes of particles coming from reservoirs to the scattering region (incoming) and particles reflecting or transmitting through the scattering region (outgoing). These incoming and outgoing particle fluxes are related linearly via the scattering matrix as follows

$$b_{\alpha n}(E) = \sum_{\beta} \sum_m s_{\alpha n, \beta m}(E) a_{\beta m}(E), \quad (4.2)$$

and in vector form as

$$\vec{b} = \hat{S} \vec{a}. \quad (4.3)$$

The element $s_{\alpha n, \beta m}(E)$ of the scattering matrix \hat{S} shows a particle to be scattered from channel m of lead β to channel n of lead α . When calculating the transport quantities in the next section, it is appropriate to define field operators. Field operators $\hat{\psi}(\mathbf{r}_{\alpha}, t)$ and $\hat{\psi}^{\dagger}(\mathbf{r}_{\alpha}, t)$, are operators that annihilate and create particles at a given point in each lead and time. In lead α we have

$$\begin{aligned} \hat{\psi}(\mathbf{r}_{\alpha}, t) &= \sum_n^{\mathcal{N}} \int \frac{dE}{\sqrt{2\pi\hbar v_{\alpha n}}} e^{-iEt/\hbar} \Phi_{\alpha n}(y_{\alpha}, z_{\alpha}) [\hat{a}_{\alpha n}(E) e^{ik_x^{\alpha n} x_{\alpha}} + \hat{b}_{\alpha n}(E) e^{-ik_x^{\alpha n} x_{\alpha}}], \\ \hat{\psi}^{\dagger}(\mathbf{r}_{\alpha}, t) &= \sum_n^{\mathcal{N}} \int \frac{dE}{\sqrt{2\pi\hbar v_{\alpha n}}} e^{iEt/\hbar} \Phi_{\alpha n}^*(y_{\alpha}, z_{\alpha}) [\hat{a}_{\alpha n}^{\dagger}(E) e^{-ik_x^{\alpha n} x_{\alpha}} + \hat{b}_{\alpha n}^{\dagger}(E) e^{ik_x^{\alpha n} x_{\alpha}}]. \end{aligned} \quad (4.4)$$

The fermionic operators, $\hat{a}_{\alpha n}(E)$ ($\hat{a}_{\alpha n}^{\dagger}(E)$) and $\hat{b}_{\alpha n}(E)$ ($\hat{b}_{\alpha n}^{\dagger}(E)$) are related by the scattering matrix defined in Eq. (4.2)

$$\hat{b}_{\alpha n}(E) = \sum_{\beta} \sum_m s_{\alpha n, \beta m}(E) \hat{a}_{\beta m}(E). \quad (4.5)$$

These fermionic operators, $\hat{a}_{\alpha n}(E)$ and $\hat{b}_{\alpha n}(E)$, obey anti-commutation relations,

$$\begin{aligned}\{\hat{a}_{\alpha n}^\dagger(E), \hat{a}_{\beta m}(E')\} &= \delta_{\alpha\beta} \delta_{nm} \delta(E - E'), \\ \{\hat{a}_{\alpha n}^\dagger(E), \hat{a}_{\beta m}^\dagger(E')\} &= 0, \\ \{\hat{a}_{\alpha n}(E), \hat{a}_{\beta m}(E')\} &= 0,\end{aligned}\tag{4.6}$$

and analogously for \hat{b} operators.

In general, a scattering matrix in a normal metal is block-diagonal and satisfies the symmetry relation

$$\hat{S}_N = \begin{pmatrix} \hat{s}_0(E) & 0 \\ 0 & \hat{s}_0(-E)^\dagger \end{pmatrix},\tag{4.7}$$

where N labels the normal metal. The two blocks correspond to the scattering matrices for electrons and holes. These blocks are not coupled in a normal metal, but they are in a superconductor as will be discussed in Sec. (3.2.1). A scattering matrix \hat{S} is a unitary matrix, $\hat{S}^{-1} = \hat{S}^\dagger$, guaranteeing current conservation at the scatterer. In the presence of a magnetic field, B , the matrix fulfills the relation $\hat{S}^T(B) = \hat{S}(-B)$ due to the time-reversal symmetry. For a two-terminal structure, $\alpha, \beta \equiv \text{L, R}$, we can represent the scattering matrix in a block structure for electrons as

$$\hat{s}_0(E) = \begin{pmatrix} \hat{s}_{\text{LL}} & \hat{s}_{\text{LR}} \\ \hat{s}_{\text{RL}} & \hat{s}_{\text{RR}} \end{pmatrix} = \begin{pmatrix} \hat{r} & \hat{t}' \\ \hat{t} & \hat{r}' \end{pmatrix},\tag{4.8}$$

where \hat{r} , (\hat{r}') is the reflection and \hat{t} , (\hat{t}') the transmission matrices.

The resulting transmission probabilities from the scattering matrix govern the charge and heat current through a junction, which we describe in the following sections.

4.2 Transport quantities

The method we use for the calculation of transport observables is the Landauer-Büttiker formalism which is based on calculating currents with the help of scattering states [102, 105, 107]. We are mainly interested in particle, charge and heat currents.

4.2.1 Charge and heat current operators

Here we give a derivation of the explicit expressions for charge and heat currents. We start by writing the charge current density, and we obtain the charge current

operator at lead α

$$\hat{I}_\alpha(x_\alpha, t) = \int dy_\alpha dz_\alpha \hat{j}_\alpha(\mathbf{r}_\alpha, t). \quad (4.9)$$

The charge current density, \hat{j} satisfies a continuity relation that guarantees charge conservation,

$$\frac{\partial \hat{\rho}}{\partial t} + \nabla \cdot \hat{j}_\alpha = 0 \quad (4.10)$$

The charge density operator, $\hat{\rho}$, is defined by the square of field operator as $\hat{\rho} = -e|\hat{\psi}|^2$. Substituting this into the continuity relation gives

$$-\frac{\partial \hat{\rho}}{\partial t} = \frac{e\partial|\hat{\psi}|^2}{\partial t} = \nabla \cdot \left[\frac{-e\hbar}{2im} [\hat{\psi}^\dagger \nabla \hat{\psi} - (\nabla \hat{\psi}^\dagger) \hat{\psi}] \right]. \quad (4.11)$$

Therefore we identify the current density as

$$\hat{j}_\alpha = \frac{e\hbar}{2im} [\hat{\psi}^\dagger \nabla \hat{\psi} - (\nabla \hat{\psi}^\dagger) \hat{\psi}]. \quad (4.12)$$

Substituting Eqs. (4.4) into Eq. (4.12) and the result into Eq. (4.9) considering the orthonormality of transverse wave functions, we obtain the charge current at lead α

$$\hat{I}_\alpha(t) = \frac{-e}{h} \sum_n^{\mathcal{N}} \int dE dE' e^{i(E-E')t/\hbar} [\hat{a}_{\alpha n}^\dagger(E) \hat{a}_{\alpha n}(E') - \hat{b}_{\alpha n}^\dagger(E) \hat{b}_{\alpha n}(E')]. \quad (4.13)$$

We attain the average charge current by taking the quantum average of Eq. (4.13). Assuming the reservoirs to be at equilibrium, we have the following relations for the average of incoming and outgoing fermionic operators,

$$\begin{aligned} \langle \hat{a}_{\alpha n}^\dagger(E) \hat{a}_{\beta m}(E') \rangle &= \delta_{\alpha\beta} \delta_{nm} \delta(E - E') f_\alpha(E), \\ \langle \hat{b}_{\alpha n}^\dagger(E) \hat{b}_{\beta m}(E') \rangle &= \sum_{\alpha', \beta'} \sum_{n', m'} s_{\alpha n, \alpha' n'}(E) s_{\beta m, \beta' m'}(E) \langle \hat{a}_{\alpha' n'}^\dagger(E) \hat{a}_{\beta' m'}(E') \rangle. \end{aligned} \quad (4.14)$$

Since the incoming states in Eq. (4.13) are distributed following the Fermi distribution, therefore

$$f_\alpha(E) = \frac{1}{1 + \exp((E - \mu_\alpha)/(k_B T_\alpha))} \quad (4.15)$$

determines the fermionic particle occupation in the lead α . Using Eqs. (4.14) we can write the charge current in Eq. (4.13) as

$$\hat{I}_\alpha(t) = \frac{-e}{h} \sum_{\beta, \gamma} \sum_{m, n} \int dE dE' e^{i(E-E')t/\hbar} [\hat{a}_{\beta m}^\dagger(E) \mathcal{A}_{\beta\gamma}^{mn}(\alpha; E, E') \hat{a}_{\gamma n}(E')], \quad (4.16)$$

where

$$\mathcal{A}_{\beta\gamma}^{mn}(\alpha; E, E') = \delta_{\alpha\beta} \delta_{\alpha\gamma} \delta_{mn} - \sum_l s_{\alpha l, \beta m}^\dagger(E) s_{\alpha l, \gamma n}(E'). \quad (4.17)$$

In case there are only two reservoirs left (L) and right (R), Eqs. (4.14) for $\alpha = L$ gives

$$\begin{aligned}\langle \hat{a}_{Ln}^\dagger(E) \hat{a}_{Ln}(E) \rangle &= f_L(E), \\ \langle \hat{b}_{Ln}^\dagger(E) \hat{b}_{Ln}(E) \rangle &= R_n f_L(E) + \mathcal{D}_n f_R(E),\end{aligned}\quad (4.18)$$

where R_n is the reflection probability of channel n in lead L and $\mathcal{D}_n = 1 - R_n$ is the transmission probability from lead R to L in channel n . Substituting this into Eq. (4.13) gives

$$I_L = \frac{-e}{h} \sum_{n=0}^{\mathcal{N}} \int dE \mathcal{D}_n [f_L(E) - f_R(E)]. \quad (4.19)$$

Here the current flows out of terminal L.

Particles (electrons and holes) carry energy as well as charge. Similar to the charge flow, we can write the continuity equation for the energy flow as $\frac{\partial \hat{\rho}^E}{\partial t} + \nabla \cdot \hat{j}_\alpha^E = \rho_S^E$ where ρ_S^E is the energy density of a source. Integrating both sides over the entire volume of the system we obtain the relation for the source

$$\rho_S^E = \hat{\psi}^\dagger(E, \mathbf{r}_\alpha) \frac{\partial U(t)}{\partial t} \hat{\psi}(E, \mathbf{r}_\alpha), \quad (4.20)$$

where $U(t)$ is a time-dependent potential we consider in the Hamiltonian of an electron. The energy current density can be written as

$$\hat{j}_\alpha^E(\mathbf{r}_\alpha, t) = \frac{\hbar^2}{2m} [\hat{\psi}^\dagger \frac{\partial \nabla \hat{\psi}}{\partial t} - (\nabla \hat{\psi}^\dagger) \frac{\partial \hat{\psi}}{\partial t}]. \quad (4.21)$$

The total energy current operator at lead α will be

$$\hat{I}_\alpha^E(x_\alpha, t) = \int dy_\alpha dz_\alpha \hat{j}_\alpha^E(\mathbf{r}_\alpha, t). \quad (4.22)$$

Substituting the field operators of Eqs. (4.4) into Eq. (4.21) and the result into Eq. (4.22) gives

$$\hat{I}_\alpha^E(t) = \frac{1}{h} \sum_n \int dE dE' \left(\frac{E + E'}{2} \right) e^{i(E-E')t/\hbar} [\hat{a}_{\alpha n}^\dagger(E) \hat{a}_{\alpha n}(E') - \hat{b}_{\alpha n}^\dagger(E) \hat{b}_{\alpha n}(E')]. \quad (4.23)$$

In addition to the energy current, we are in particular interested in heat currents. The extra energy current with respect to Fermi level is defined as heat current, and it can be expressed in terms of particle and energy currents as follows,

$$\hat{J}_\alpha = \hat{I}_\alpha^E - \frac{\mu_\alpha}{e} \hat{I}_\alpha, \quad (4.24)$$

where μ_α denotes the equilibrium electrochemical potential of lead α . Similar to the charge current as in Eq. (4.19), the average heat current flowing out of terminal L for the two-terminal case is

$$J_L = \frac{1}{h} \sum_{n=0}^{\mathcal{N}} \int dE (E - \mu_L) \mathcal{D}_n [f_L(E) - f_R(E)]. \quad (4.25)$$

4.2.2 Linear response: charge and heat conductances

In chapter 3, in the Onsager relation section, charge and heat conductances were introduced. To achieve the charge and heat conductance in a normal metal, we employ the linear response approximation. In order to be in the linear response regime, we need the voltage and temperature gradients applied through the system to be small compared to the temperatures of the system. Applying voltage and temperature biases through a system drives charge and heat currents. We consider the applied voltage V_α and temperature biases ΔT_α as terms added to the equilibrium values of chemical potential and temperature such as $T_\alpha = T + \Delta T_\alpha$ and $\mu_\alpha = \mu - eV_\alpha$. If these biases are small compared to the equilibrium values then the linear response occurs. These biases enter the charge and heat currents through Fermi function. Expanding the Fermi function of Eq. (4.15) around these values gives

$$\begin{aligned} f_\alpha(E) &\approx f(E) + \frac{\partial f}{\partial T} \Delta T_\alpha + \frac{\partial f}{\partial \mu} (eV_\alpha) \\ &= f(E) - \frac{\partial f}{\partial E} \left[\frac{(E - \mu) \Delta T_\alpha}{T} + eV_\alpha \right], \end{aligned} \quad (4.26)$$

where $\partial f / \partial E = -1/4k_B T \cosh^2[(E - \mu)/2k_B T]$ is the derivative of Fermi function with respect to energy. Substituting the expansion of Eq. (4.26) into the expressions for charge and heat currents, average of Eqs. (4.19) and (4.25) gives charge and heat conductances.

In the absence of a temperature gradient, $\Delta T = 0$, using Eq. (4.19) for an energy independent transmission \mathcal{D}_n and taking V in the first order we have

$$G = \left. \frac{\partial I_\alpha}{\partial V_\beta} \right|_{\{V\}=0} = G_0 \sum_{n=0}^{\mathcal{N}} \mathcal{D}_n, \quad (4.27)$$

where $G_0 = e/h$ is the charge conductance quantum.

In the absence of voltage gradient for a two-terminal conductor and assuming the temperature gradient of ΔT between the two terminals left and right we approximate the difference of Fermi functions as

$$f_L(E) - f_R(E) \approx -\frac{\partial f}{\partial E} (E - \mu) \frac{\Delta T}{T}. \quad (4.28)$$

Inserting this into Eq. (4.25) we consequently obtain

$$J(T) \approx -\frac{k_B^2 T}{h} \sum_{n=0}^{\mathcal{N}} \mathcal{D}_n \int_0^\infty dE \left(\frac{E - \mu}{k_B T} \right)^2 \frac{\partial f}{\partial E} \Delta T. \quad (4.29)$$

We considered the transmission eigenvalues \mathcal{D}_n to be energy independent. Such an assumption allows for calculating analytically the energy integral in the equa-

tion above, yielding

$$\int_0^\infty dE \left(\frac{E - \mu}{k_B T} \right)^2 \frac{\partial f}{\partial E} = -\frac{\pi^2}{3}. \quad (4.30)$$

As a result, the heat current in the linear response regime takes the form

$$J(T) = \frac{\pi^2 k_B T}{3h} \sum_{n=0}^{\mathcal{N}} \mathcal{D}_n \cdot \Delta T \equiv \kappa_{\mathcal{N}}(T) \cdot \Delta T. \quad (4.31)$$

The heat conductance of a normal metal $\kappa_{\mathcal{N}}(E)$ corresponds simply to the heat conductance quantum, defined as $\kappa_0 = \pi^2 k_B T / (3h)$, multiplied by the sum over transmission eigenvalues. The charge and heat conductances are related by Wiedemann-Franz law, as introduced in chapter 3.

4.2.3 Charge and heat current noise

Together with the average currents, noise in charge and heat currents gives us additional information about transport such as the charge of the current carriers. An example is that noise measurements were used to prove that the charge carriers are fractionally charged in the fractional quantum Hall states [108]. Two types of noises that exist in the kind of systems we study are thermal and shot noises [109, 110]. Thermal noise always exists in mesoscopic conductors with finite temperatures. Thermal agitation of the charge carriers causes fluctuations of the occupation number of the states of the system. The occupation number fluctuations lead to equilibrium current fluctuations, which are related to the conductance of the system via the fluctuation-dissipation theorem. The fluctuation-dissipation theorem quantifies the relation between thermal fluctuations and the response of the system. While thermal noise is present in the system's equilibrium state, when the system is driven out of equilibrium, another type of noise arises that is called shot noise. Shot noise originates from the quantized nature of charge.

Charge current noise has been long calculated [110]. In order to calculate the current fluctuations, a correlation function of the currents in two leads α and β at times t and t' is defined as

$$\mathcal{S}_{\alpha\beta}(t - t') = \frac{1}{2} \langle \Delta \hat{I}_\alpha(t) \Delta \hat{I}_\beta(t') + \Delta \hat{I}_\beta(t') \Delta \hat{I}_\alpha(t) \rangle. \quad (4.32)$$

The Fourier transform of this correlation is known as noise power.

$$2\pi\delta(\omega + \omega') S_{\alpha\beta}(\omega) = \langle \Delta \hat{I}_\alpha(\omega) \Delta \hat{I}_\beta(\omega') + \Delta \hat{I}_\beta(\omega') \Delta \hat{I}_\alpha(\omega) \rangle, \quad (4.33)$$

where $\Delta \hat{I}_\alpha(\omega) = \hat{I}_\alpha(\omega) - \langle \hat{I}_\alpha(\omega) \rangle$ and

$$\langle \Delta \hat{I}_\alpha(\omega) \Delta \hat{I}_\beta(\omega') \rangle = \langle \hat{I}_\alpha(\omega) \hat{I}_\beta(\omega') \rangle - \langle \hat{I}_\alpha(\omega) \rangle \langle \hat{I}_\beta(\omega') \rangle. \quad (4.34)$$

Using Eq. (4.13), the Fourier transform of the current operator, $\hat{I}_\alpha(\omega)$ is

$$\hat{I}_\alpha(\omega) = \frac{e}{\hbar} \sum_{\beta, \gamma} \sum_{m, n} \int dE [\hat{a}_{\beta m}^\dagger(E) \mathcal{A}_{\beta\gamma}^{mn}(\alpha; E, E + \hbar\omega) \hat{a}_{\gamma n}(E + \hbar\omega)]. \quad (4.35)$$

To calculate the average product of currents in Eq. (4.34) we use Eqs. (4.16) together with the average of the products of four Fermionic operators

$$\begin{aligned} & \langle \hat{a}_{\alpha n}^\dagger(E_1) \hat{a}_{\beta m}(E_1) \hat{a}_{\alpha' n'}^\dagger(E_2) \hat{a}_{\beta' m'}(E_2) \rangle - \langle \hat{a}_{\alpha n}^\dagger(E_1) \hat{a}_{\beta m}(E_1) \rangle \langle \hat{a}_{\alpha' n'}^\dagger(E_2) \hat{a}_{\beta' m'}(E_2) \rangle \\ & = \delta_{\alpha\beta'} \delta_{\beta\alpha'} \delta_{nm'} \delta_{mn'} \delta(E_1 - E_2) \delta(E_1' - E_2) f_\alpha(E_1) [1 - f_\beta(E_2)]. \end{aligned} \quad (4.36)$$

Substituting the averages of currents into Eq. (4.33) we obtain the charge current noise

$$\begin{aligned} \mathcal{S}_{\alpha\beta}(\omega) &= \frac{e^2}{\hbar} \sum_{\alpha', \beta'} \sum_{n' m'} \int dE \text{Tr}[\mathcal{A}_{\alpha'\beta'}^{n' m'}(\alpha; E, E + \hbar\omega) \mathcal{A}_{\beta'\alpha'}^{m' n'}(\beta; E + \hbar\omega, E)] \\ & \quad \times \{f_{\alpha'}(E)[1 - f_{\beta'}(E + \hbar\omega)] + f_{\beta'}(E)[1 - f_{\alpha'}(E + \hbar\omega)]\}, \end{aligned} \quad (4.37)$$

The zero-frequency limit of charge current noise is

$$\begin{aligned} \mathcal{S}_{\alpha\beta} &= \frac{e^2}{\hbar} \sum_{\alpha', \beta'} \sum_{n' m'} \int dE \text{Tr}[\mathcal{A}_{\alpha'\beta'}^{n' m'}(\alpha; E) \mathcal{A}_{\beta'\alpha'}^{m' n'}(\beta; E)] \\ & \quad \times \{f_{\alpha'}(E)[1 - f_{\beta'}(E)] + f_{\beta'}(E)[1 - f_{\alpha'}(E)]\}. \end{aligned} \quad (4.38)$$

In the two-terminal case the charge current noise is

$$\begin{aligned} \mathcal{S} &= \frac{2e^2}{h} \sum_n \int dE \{ \mathcal{D}_n [f_L(E)(1 - f_L(E)) + f_R(E)(1 - f_R(E))] \\ & \quad + \mathcal{D}_n(1 - \mathcal{D}_n)(f_L - f_R)^2 \}. \end{aligned} \quad (4.39)$$

Starting from Eq. (4.32) and following the same procedure as charge current noise for heat currents we reach to heat current fluctuations. In zero frequency we have

$$\begin{aligned} \mathcal{S}_{\alpha\beta}^J &= \frac{1}{h} \sum_{\alpha', \beta'} \sum_{n' m'} \int dE E^2 \text{Tr}[\mathcal{A}_{\alpha'\beta'}^{n' m'}(\alpha; E) \mathcal{A}_{\beta'\alpha'}^{m' n'}(\beta; E)] \\ & \quad \times \{f_{\alpha'}(E)[1 - f_{\beta'}(E)] + f_{\beta'}(E)[1 - f_{\alpha'}(E)]\}. \end{aligned} \quad (4.40)$$

We will use the heat current noise in the continuation of papers III and IV.

4.3 Superconducting systems

After reviewing the scattering formalism for heat transport in a normal metal, we introduce the scattering formalism for a superconductor, and we show the scattering behavior of transport channels in superconductors.

4.3.1 Scattering theory for superconductors

Using the Landauer formula for heat currents in a superconductor, as shown in detail in the Licentiate thesis [111], we obtain

$$\hat{J}_\alpha^S(t, T) = \frac{1}{\hbar} \sum_n^{\mathcal{N}} \sum_{i=e,h} \int_{\max(\Delta)}^{\infty} dE dE' e^{i(E-E')t/\hbar} \times \left(\frac{E + E'}{2} \right) \left[\hat{b}_{\alpha n, i}^\dagger(E) \hat{b}_{\alpha n, i}(E') - \hat{a}_{\alpha n, i}^\dagger(E) \hat{a}_{\alpha n, i}(E') \right]. \quad (4.41)$$

In the expression above, there are two parts for electron- ($i = e$) and hole-like ($i = h$) quasiparticle contributions to the heat current with a sum over \mathcal{N} transport eigenchannels in a superconducting lead. The gap Δ in the lower limit of integration should be understood as the maximum gap in the case we have different superconducting leads with unequal gap functions. Here, the operators $\hat{a}_{i,n}^{(\dagger)}$ ($\hat{a}_{i,n}$) and $\hat{b}_{i,n}^{(\dagger)}$ ($\hat{b}_{i,n}$) represent incoming and outgoing states to the superconductor's junction with the scatterer and in this case they indicate Bogoliubov operators. As mentioned before, the incoming and outgoing states are related to each other by a scattering matrix specific to the junction under consideration. Here, the electrochemical potential is set to $\mu_\alpha = 0$. Analogous to normal metal, the heat-current for a two-terminal case is shown as the following expression,

$$J_L^S(T) = \frac{1}{\hbar} \sum_{n=0}^{\mathcal{N}} \int_{\max(\Delta)}^{\infty} dE E [\mathcal{D}_n^e + \mathcal{D}_n^h] [f_L(E) - f_R(E)]. \quad (4.42)$$

The Fermi functions $f_\alpha(E)$ here determine the quasiparticle occupations in superconducting contacts, $\alpha \equiv L, R$. The transmission probability of channel n consists of electron-like and hole-like quasiparticles contributions that are equal due to particle-hole symmetry ($\mathcal{D}_n^e = \mathcal{D}_n^h$). The transmission probability \mathcal{D}_n^e is a sum of transmission probabilities of electron-like and hole-like quasiparticles to the electron-like channels, $\mathcal{D}_n^e = \mathcal{D}_n^{ee} + \mathcal{D}_n^{eh}$. These transmission probabilities are calculated using scattering matrices for NS and different regimes of SNS junctions in the next sections. These transmission probabilities in superconductors are energy-dependent, and the dependence of heat currents and transport properties to parameters such as the superconducting phase is through these transmissions.

In order to attain the linear response heat conductances in a superconductor, we use Eq. (4.26) as in normal metal and substitute that into Eq. (4.42). Employing this we obtain

$$\kappa^S(T) = \frac{1}{2\hbar} \sum_{n=0}^{\mathcal{N}} \frac{1}{k_B T^2} \int_{\Delta}^{\infty} dE \frac{E^2}{\cosh^2(E/(2k_B T))} \mathcal{D}_n^e. \quad (4.43)$$

Here, we also made use of the particle-hole symmetry which means that the transmission probabilities of electron-like (\mathcal{D}_n^e) and hole-like (\mathcal{D}_n^h) quasiparticles are equal.

The next quantity we will consider to study in the continuation of paper IV (this is not part of paper IV currently) is the heat current noise in a superconducting lead. Following the same approach we used for normal metal, we obtain the zero frequency heat current noise in a superconductor as

$$\begin{aligned} \mathcal{S}_{\alpha\beta}^J = & \frac{1}{h} \sum_{\alpha',\beta'} \sum_{n'm'} \int_{\max(\Delta)}^{\infty} dE E^2 \text{Tr}[\mathcal{A}_{\alpha'\beta'}^{n'm'}(\alpha; E) \mathcal{A}_{\beta'\alpha'}^{m'n'}(\beta; E)] \\ & \times \{f_{\alpha'}(E)[1 - f_{\beta'}(E)] + f_{\beta'}(E)[1 - f_{\alpha'}(E)]\}, \end{aligned} \quad (4.44)$$

where $\mathcal{A}_{\alpha'\beta'}^{n'm'}(\alpha; E)$ is given by Eq. (4.17).

4.4 Transmission probabilities for specific devices

In this section, we review the transmission functions of nanostructures for which we study the thermoelectric performance in papers II and III. As we saw in the previous sections, to study the transport properties using scattering theory, the transmission probability of the nanostructure is needed. These nanostructures include a single level quantum dot, a rectangular barrier, a quantum spin Hall system where backscattering is induced by a magnetic moment, and a quantum point contact.

4.4.1 Transmission probability for a single level system with Lorentzian shape

In chapter 3, we introduced quantum dot as an artificially made system where electrons are confined and occupy discrete levels. To keep the levels discrete, the quantum dot states should be well isolated by the surrounding gates [74]. Here we assume that this condition is fulfilled. To use the scattering matrix for a quantum dot, we use the results of a formalism that relates the scattering matrix of the dot to its effective Hamiltonian, as suggested in [78, 112, 113]. This relation is given as

$$\mathcal{S}(E) = \mathbf{1} - 2\pi i W^\dagger \frac{1}{E - H_{\text{eff}}} W, \quad (4.45)$$

where $H_{\text{eff}} = H_{\text{dot}} - i\pi W W^\dagger$. The dot's Hamiltonian is H_{dot} and $\Gamma = 2\pi W W^\dagger$ is called the width matrix with W being the coupling of reservoir modes to dot

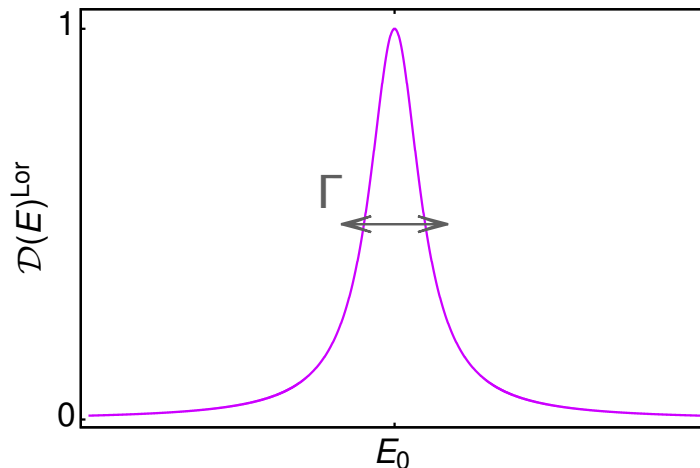


Figure 4.2: Transmission probability for a quantum dot, as defined in Eq. (4.47) with $\Gamma_L = \Gamma_R = \Gamma/2$.

states. Considering two single mode reservoirs L and R coupled to a single state dot, we have $W = (w_L, w_R)$ which gives

$$\mathcal{S}(E) = \begin{pmatrix} 1 & 0 \\ 0 & 1 \end{pmatrix} - \frac{2\pi i}{E - E_0 + \frac{i}{2}(\Gamma_L + \Gamma_R)} \begin{pmatrix} w_L^* w_L & w_L^* w_R \\ w_R^* w_L & w_R^* w_R \end{pmatrix}. \quad (4.46)$$

Having the scattering matrix we know that the probability of going from reservoir α to β is $\mathcal{D}_{\alpha\beta}(E) = |S_{\alpha,\beta}(E)|^2$. Since there is only a single mode, the transmission function will be the same as this probability. Substituting Eq. (4.46) into $\mathcal{D}_{\alpha\beta}(E)$ we obtain the transmission probability of the single-level quantum dot from right to left reservoir as

$$\mathcal{D}_{\text{LR}}^{\text{Lor}}(E) = \frac{\Gamma_L \Gamma_R}{(E - E_0)^2 + \frac{1}{4}(\Gamma_L + \Gamma_R)^2}, \quad (4.47)$$

where as mentioned $\Gamma_\alpha = 2\pi|w_\alpha|^2$ with $\alpha = L, R$, with Γ_α/\hbar being the tunneling rate. We see that this transmission has a Lorentzian dependence on energy, see Fig. (4.2).

4.4.2 Transmission probability for a rectangular barrier

Another transmission we address here is the one resulting from a rectangular barrier potential. Consider a one-dimensional potential barrier of height V and spatial extension L_V , given by

$$V(x) = \begin{cases} V & \text{for } 0 \leq x \leq L_V \\ 0 & \text{for } |x| \geq L_V \end{cases} \quad (4.48)$$

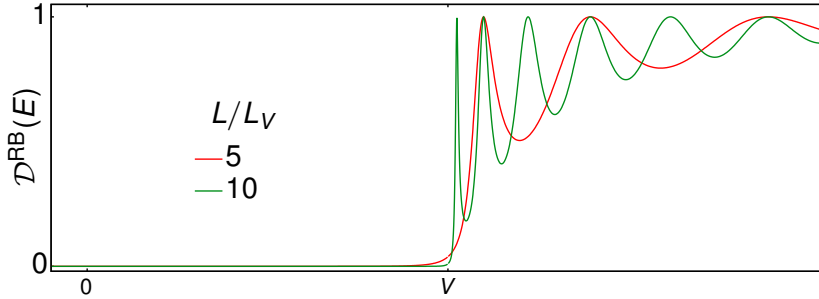


Figure 4.3: Transmission probability for the rectangular barrier, as defined in Eq. (4.49).

For energies $E < V$, an incident particle to the barrier from one side, can be either reflected or transmitted. Writing Schrödinger equation for the incident wave from left and solving the boundary conditions for the wave functions, we attain the reflection and transmission amplitudes. The result is

$$\mathcal{D}^{\text{RB}}(E) = \frac{1}{1 + \frac{V^2}{4E|E-V|} \sin^2(kL_V)}, \quad (4.49)$$

where $k = \sqrt{2m|E - V|/\hbar^2}$. This transmission function exponentially decays with the barrier width, and outside the barrier, it oscillates. These oscillations resemble the peak-shaped transmission of a quantum dot. We will see similar behavior in the QSH transmission in the next section. At $E = V$ the transmission probability is

$$\mathcal{D}^{\text{RB}}(E = V) = \frac{1}{1 + 2mL_V^2 V/\hbar^2}. \quad (4.50)$$

4.4.3 Transmission probability for a quantum point contact

As we stated in chapter 3, a QPC is a constriction created by gate voltages in a nanostructure. Many transport channels arrive at the point contact, and only a finite number of them are transmitted. Particles arriving at the point contact are hence reflected or transmitted. When the constriction of QPC is induced electrostatically, one can consider a smooth pattern for the narrowest point, as suggested in [114]: a saddle point function can approximate the potential in the plane of two-dimensional electron gas ($x - y$ plane)

$$V(x, y) = V_0 - \frac{1}{2}m\omega_x^2 x^2 + \frac{1}{2}m\omega_y^2 y^2, \quad (4.51)$$

where x is the longitudinal direction along the QPC between two reservoirs, and y is the transverse direction. V_0 is the potential at the saddle, and ω_x and ω_y

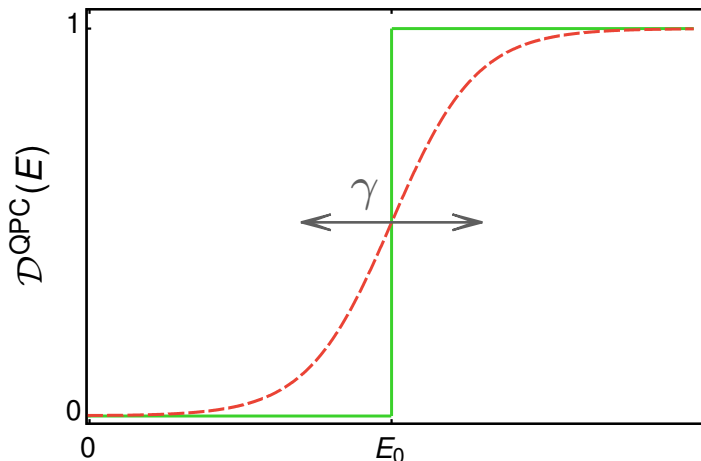


Figure 4.4: Transmission probability for the QPC device, as defined in Eq. (4.53).

are the angular frequencies. Solutions of energies for the transverse direction are the same as a quantum harmonic oscillator,

$$E_n = V_0 + \hbar\omega_y \left(n + \frac{1}{2} \right). \quad (4.52)$$

Here, n indicates the number of channels. The transmission probability of the above-stated potential is found to be

$$\mathcal{D}^{\text{QPC}}(E) = \sum_n \frac{1}{1 + e^{(-E+E_n)/\gamma}}. \quad (4.53)$$

Plotting this transmission function for a single channel with $n = 0$ gives a step-like plot, Fig. (4.4) where $\gamma = \hbar\omega_x/2\pi$ indicates the smoothness of the step. When $\omega_x \rightarrow 0$ and therefore $\gamma \rightarrow 0$, the point contact is very long and the transmission simplifies to the sharp step that is described by the Heaviside function $\mathcal{D}^{\text{step}}(E) = \sum_n \Theta(E - E_n)$.

4.4.4 Transmission probability for a quantum spin Hall system

In this section, we consider a quantum spin Hall (QSH) device, which is the main focus of paper II. As mentioned in paper II, we assume QSH edge states coupled to a magnetic domain with length L , see Fig. (4.5), as suggested in [26]. The following Hamiltonian models such a system

$$H = \int dx \Psi^\dagger(x) [(-i\hbar v_F \partial_x) \sigma_z + J \mathbf{M}(x) \cdot \hat{\boldsymbol{\sigma}}] \Psi(x), \quad (4.54)$$

where $\Psi(x) = (\psi_{+,\uparrow}, \psi_{-,\downarrow})^T$ indicate chiral right (+) and left (-) moving particles with spins up and down. J is the magnetic exchange interaction of magnetic

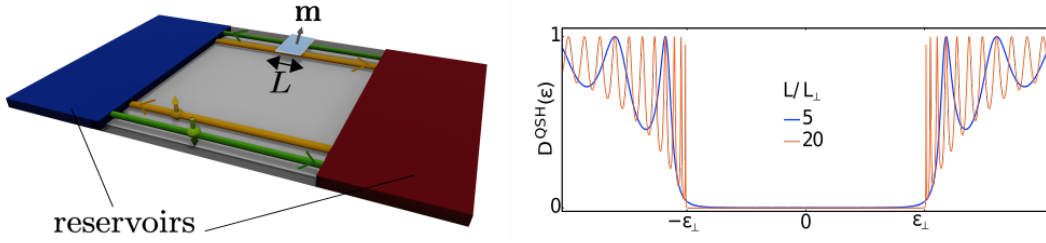


Figure 4.5: *Left: QSH device with a magnetic island. Right: transmission probability for the QSH device, as defined in Eq. (4.56).*

moment and spin of particles and $\hat{\boldsymbol{\sigma}} = (\sigma_x, \sigma_y, \sigma_z)$ are the Pauli matrices. The magnetic moment of the island is represented by the function $\mathbf{M}(x) = \Theta(L - x)\Theta(x)\mathbf{m}$ with the magnetic moment unit $\mathbf{m} = (m_\perp \cos \phi, m_\perp \sin \phi, m_\parallel)$ where m_\perp and m_\parallel are the perpendicular and parallel components to the spin-orbit interaction.

Far away from the magnetic moment, the edge states propagate freely and are eventually injected or absorbed by electrodes. In the scattering region of the magnetic coupling, a backscattering at the same edge is enabled by spin flips. For this scattering region, as suggested in [96], an evolution operator between the channels in the same edge can be written as

$$\hat{U}(L) = \exp\left(i\frac{\epsilon_\parallel}{\hbar v_F}L\right)\left[\sigma_x \cos \lambda - i\frac{\hat{\boldsymbol{\lambda}}}{\lambda} \cdot \hat{\boldsymbol{\sigma}} \sin \lambda\right], \quad (4.55)$$

where $\hat{\boldsymbol{\lambda}} = (i\epsilon_\perp \sin \phi, -i\epsilon_\perp \cos \phi, \epsilon)L/\hbar v_F$ with $\epsilon_{\perp(\parallel)} = Jm_{\perp(\parallel)}$. Using \hat{U} one can calculate the transmission function as the inverse of the matrix \hat{U} . The result for a single magnetic domain is

$$\mathcal{D}^{\text{QSH}}(\epsilon) = \frac{|\epsilon_\perp^2 - \epsilon^2|}{|\epsilon_\perp^2 - \epsilon^2| \cos^2(rl) + \epsilon^2 \sin^2(rl)}, \quad (4.56)$$

with $l = L/L_\perp$, $L_\perp = \hbar v_F/\epsilon_\perp$ and $r = \sqrt{(\epsilon/\epsilon_\perp)^2 - 1}$. The behavior of the transmission probability in Eq. (4.56) is shown in Fig. (4.5) for different lengths of the magnetic island. As we see there are similarities to the quantum dot and QPC transmissions due to the oscillations and the step-like behavior. Despite the similarities to the transmission of rectangular barrier, due to the quadratic dispersion of the free electronic quasiparticles in the rectangular barrier above the band bottom, the transmission of rectangular barrier has only a single step at positive energies.

4.5 Scattering matrix for composed systems

4.5.1 Scattering matrix for an SNS junction

In paper I, we study heat transport in a superconductor-normal metal-superconductor (SNS) junction. Here, we explain the construction of the scattering matrix of this junction. The model we consider for the junction consists of a normal region containing a generic barrier or a disordered part between two superconducting regions S_L and S_R . This model is illustrated in figure (4.6).

The construction of the scattering matrix of the SNS junction is explained in details in the Licentiate thesis [111]. There, the BdG equation is used together with wave function matching to obtain the scattering matrix. The considered model is valid in superconductor clean limit where the quasiparticle mean free path l is large compared to the superconducting coherence length ξ ($l \gg \xi$). For a Josephson junction shown in figure (4.6) containing a disordered normal region the scattering matrix has the following structure

$$S_{\text{SNS}} = U^{-1}(\mathbf{1} - M)^{-1}(\mathbf{1} - M^\dagger)S_{\text{N}}U. \quad (4.57)$$

This matrix is written in terms of the normal scattering matrix, S_{N} . Here, we consider a multi-channel case. Having the normal scattering matrix, we can study the properties of the whole SNS junction. In the derivation of this scattering matrix, we used the trick from Ref. [115] that is, we considered a generic barrier in the middle of the normal part. The matrices in the formula (4.57) are defined as follows

$$U \equiv \begin{bmatrix} \nu & 0 \\ 0 & \nu^* \end{bmatrix}, \quad \nu \equiv \begin{bmatrix} \frac{e^{i\varphi_L/2}}{\cos \alpha_L} & \mathbf{0} \\ \mathbf{0} & \frac{e^{i\varphi_R/2}}{\cos \alpha_R} \end{bmatrix}, \quad (4.58)$$

The matrix U is a unitary matrix and contains the terms that vanish when calculating transmission probabilities using the scattering matrix. The phases of matrix U disappear due to the multiplication of the unitary matrix by its inverse. Therefore, this matrix U does not affect the final transmissions related to transport properties. Calculating the transmission probabilities from S_{SNS} shows that the phase dependence of them is due to Andreev reflection. It enters the scattering matrix via r_A that is defined as follows

$$M \equiv S_{\text{N}} \begin{bmatrix} 0 & r_A \\ r_A^* & 0 \end{bmatrix}, \quad r_A \equiv \begin{bmatrix} \sin \alpha_L e^{i\varphi_L} & \mathbf{0} \\ \mathbf{0} & \sin \alpha_R e^{i\varphi_R} \end{bmatrix}. \quad (4.59)$$

Here r_A contains the terms which are the results of Andreev scattering, where we defined $\sin \alpha_{L(R)} = v_{L(R)}/u_{L(R)}$, $u_{L(R)} = \sqrt{\Delta_{L(R)}/2E} e^{\text{arcosh}(E/\Delta_{L(R)})/2}$ and

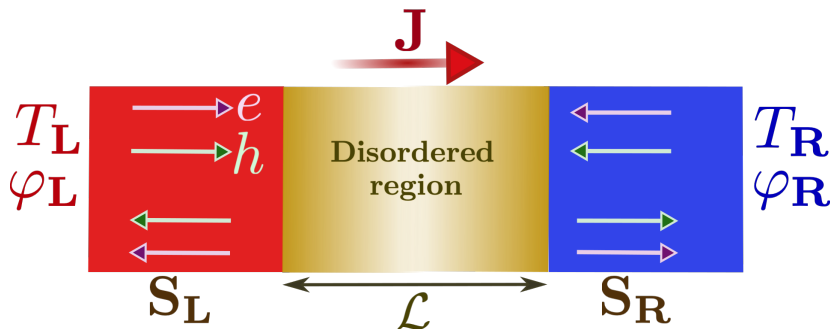


Figure 4.6: Sketch of an SNS junction across which a temperature as well as a phase difference occurs. The normal part of the junction has length \mathcal{L} and supports \mathcal{N} scattering channels. We consider the normal region to be disordered.

$v_{L(R)} = \sqrt{\Delta_{L(R)}/2E} e^{-\text{arcosh}(E/\Delta_{L(R)})/2}$. The temperature dependent gaps of the left and right superconducting leads are $\Delta_{L(R)}$.

From the scattering matrix (4.57), we obtain the transmission probability through the SNS junction needed for the calculation of heat transport quantities, namely heat current and heat conductance introduced earlier in the present chapter. The full transmission probability is a sum over transmissions of \mathcal{N} transport channels, D_n . We are interested in this summation since in paper I, we study the average of transport quantities over many channels. The transmission probabilities into the electron-like quasiparticle channel are the sum of transmissions from electron- and hole-like quasiparticles, $\mathcal{D}_n^{ee} + \mathcal{D}_n^{eh}$. They are given by

$$\mathcal{D}_n^e(E) = 2D_n \xi_L \xi_R \frac{D_n \xi_L \xi_R + (2 - D_n)(E^2 - \Delta_L \Delta_R \cos \varphi)}{((2 - D_n) \xi_L \xi_R + D_n(E^2 - \Delta_L \Delta_R \cos \varphi))^2}, \quad (4.60)$$

where $\xi_{L(R)} = \sqrt{E^2 - \Delta_{L(R)}^2}$ is the quasiparticle energy in the contact L(R). The phase difference between left and right superconductors is $\varphi = \varphi_L - \varphi_R$. Heat currents we study in superconducting junctions in paper I depend on this phase difference. This transmission is important since it is the general transmission which is valid for the case of different superconducting gaps $\Delta_L \neq \Delta_R$, and it supports different limits of D_n , including arbitrarily strong normal transmissions.

When the temperature difference of the two superconductors in Fig. (4.6) is small, the temperature dependence of the energy gap of the two leads will be equal, $\Delta_L = \Delta_R = \Delta$. The transmission probability in this case is

$$\mathcal{D}_n^e = \frac{(E^2 - \Delta^2)}{(E^2 - E_b^2)} [D_n(E^2 - \Delta^2 \cos \varphi) - D_n^2 \Delta^2 \sin^2(\varphi/2)]. \quad (4.61)$$

Here, $E_b = \Delta \sqrt{1 - D_n \sin^2(\varphi/2)}$ is the Andreev bound state energy. Multiple Andreev reflections lead to the formation of sub-gap states, called Andreev

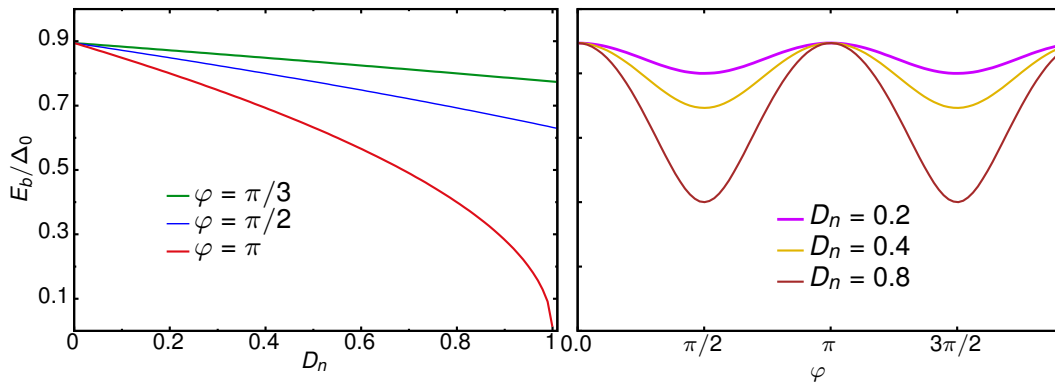


Figure 4.7: Phase and transmission dependence of the Andreev bound state energy. The temperature is $T/T_{\text{crit}} = 0.2$ and Δ_0 is the superconducting energy gap at zero temperature.

bound states, with energies below the superconducting gap. These states influence the transmissions above the gap. In Fig. (4.7) dependence of this energy on the transmission D_n and phase is shown at the temperature $T/T_{\text{crit}} = 0.2$. It is visible from the plots that the bound state energy has significant temperature and phase dependence, which influences the heat conductance. This influence is missing in the weak coupling regime where D_n is small.

In the case when there is no phase difference between superconducting leads, $\varphi = 0$, as well as the case of zero gap function, $\Delta = 0$, we obtain the transmission (4.61) which is equal to the normal transmission, $\mathcal{D}_n^e = D_n$.

4.5.2 Scattering matrix for a complex system (ring structure)

In paper IV, we study a setup as a heat circulator which consists of a three-terminal junction with normal or superconducting contacts and a central scattering region. The minimal model described in Refs. [40, 116] motivates the model of our system. In this model, the central scatterer is a non-superconducting, ring-shaped device through which a magnetic flux passes. Here, we review the construction of the scattering matrix of this setup.

As suggested and proved in Ref. [74], scattering matrix of a general multi-terminal structure with a central scatterer connected to all terminals is given by

$$S = \mathbf{r} + \mathbf{t}' \mathbf{s}^0 (1 - \mathbf{r}' \mathbf{s}^0)^{-1} \mathbf{t}, \quad (4.62)$$

with \mathbf{s}^0 being the scattering matrix of the central region. Considering a three-terminal structure with the three contacts coupled to the central ring to be superconducting, we obtain the reflection and transmission matrices, \mathbf{r}^α (\mathbf{r}'^α)

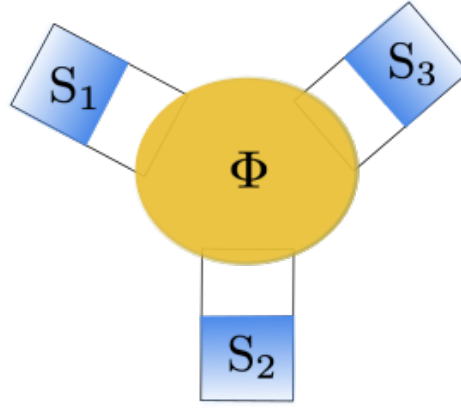


Figure 4.8: Schematic of a three-terminal setup with superconducting contacts, and penetrated by a magnetic flux Φ .

and \mathbf{t}^α (\mathbf{t}'^α), using BdG equations and wave function matching in a normal-superconductor interface, as stated in the previous section for SNS junction. The results are

$$\begin{aligned} \mathbf{r} &= \begin{bmatrix} \mathbf{0} & r_{eh} \\ r_{he} & \mathbf{0} \end{bmatrix}, & \mathbf{r}' &= \begin{bmatrix} \mathbf{0} & r'_{eh} \\ r'_{he} & \mathbf{0} \end{bmatrix}, \\ \mathbf{t} &= \begin{bmatrix} t_{ee} & \mathbf{0} \\ \mathbf{0} & t_{hh} \end{bmatrix}, & \mathbf{t}' &= \begin{bmatrix} t'_{ee} & \mathbf{0} \\ \mathbf{0} & t'_{hh} \end{bmatrix}, \end{aligned} \quad (4.63)$$

where the 3×3 reflection and transmission matrices in a normal-superconductor interface are

$$\begin{aligned} r_{eh} &= r_{he} = \text{diag}\left(\frac{-v_\alpha}{u_\alpha}\right), \\ r'_{eh} &= (r'_{he})^* = \text{diag}\left(\frac{v_\alpha}{u_\alpha} e^{i\varphi_\alpha}\right), \\ t_{ee} &= (t'_{ee})^* = (t_{hh})^* = t'_{hh} = \text{diag}\left(\frac{\sqrt{u_\alpha^2 - v_\alpha^2}}{u_\alpha} e^{i\varphi_\alpha/2}\right). \end{aligned} \quad (4.64)$$

In the previous section u_α and v_α were introduced. Here, φ_α indicates the superconducting phase.

An approach suggested in Refs. [112, 116] can be used to derive the scattering matrix of the central region from the Hamiltonian of the system. This is similar to the approach in section (4.4.1), where one can obtain the scattering matrix by solving the Schrödinger equation and relating the incoming and outgoing amplitudes to the scattering region. Following this, the scattering matrix can be written as

$$\mathbf{s}^0 = \left(\mathbf{1} - i\frac{\mathbf{W}}{2\hbar v}\right)^{-1} \left(\mathbf{1} + i\frac{\mathbf{W}}{2\hbar v}\right), \quad (4.65)$$

where \mathbf{W} contains the coupling terms between sites in the scattering region and has the form

$$\mathbf{W} = \begin{pmatrix} U_1 & t_{12}e^{-i\alpha/3} & t_{13}e^{i\alpha/3} \\ t_{12}e^{i\alpha/3} & U_2 & t_{23}e^{-i\alpha/3} \\ t_{13}e^{-i\alpha/3} & t_{23}e^{i\alpha/3} & U_3 \end{pmatrix}. \quad (4.66)$$

The effect of the magnetic flux, Φ enters the coupling matrix as $2\pi\alpha = \Phi/\Phi_0$ with the flux quantum being $\Phi_0 = h/e$.

With the elements we have now, we obtain the full scattering matrix of a three-terminal junction with superconducting leads and a central scattering region

$$S = \mathbf{r} + \mathbf{t}'S_{\text{N}}(1 - \mathbf{r}'S_{\text{N}})^{-1}\mathbf{t}, \quad (4.67)$$

where the scattering matrix of the central region in electron and hole space is

$$S_{\text{N}} = \begin{bmatrix} s^0(E) & 0 \\ 0 & s^0(-E)^\dagger \end{bmatrix}. \quad (4.68)$$

5 Exploiting specific characteristics of mesoscopic devices to control heat

The focus of this chapter is describing the specific quantum and confinement effects that we use to control and exploit heat. In paper II, energy filtering barriers are used to perform thermoelectric cooling. Paper III takes advantage of a nonequilibrium distribution as a novel resource to achieve cooling or produce power in a multi-terminal setup. Finally, in papers I and IV, the phase-coherent control of heat transport in hybrid structures of normal- and superconductors is investigated. All the papers provide analyses of the operation of experimentally accessible devices. This chapter aims to give an overview of the previous research and experiments exploiting these or similar features and their relevance to our work in the appended papers.

5.1 Thermoelectric cooling

In paper II, we use thermoelectric properties to perform cooling in a mesoscopic conductor based on a quantum spin Hall (QSH) device. We are particularly concerned with devices with energy-dependent transmission probabilities. In order to get a non-vanishing thermoelectric effect, an energy-dependent transmission probability is needed. This is shown in the following formula that a voltage gradient leads to a nonzero heat current with an energy-dependent transmission $\mathcal{D}(E)$

$$J = \frac{e}{h} \int_0^\infty dE (E - \mu) \left(\frac{-\partial f}{\partial E} \right) \mathcal{D}(E) \Delta V. \quad (5.1)$$

In this context, two classes of devices that often play a role are based on quantum point contacts (QPCs) and quantum dots (QDs). The transmissions of these systems serve as energy filters for the transfer of carriers in a specific window of energy.

QPC is the first nanostructure for which thermoelectric effects were observed experimentally [117]. It has a step-type transmission that can be used as a

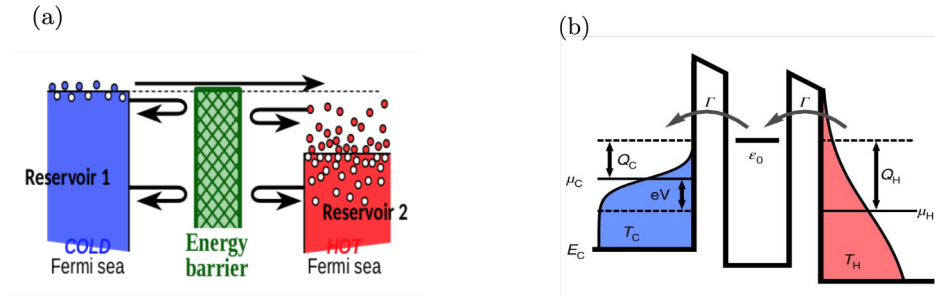


Figure 5.1: (a) Sketch of a barrier (QPC) acting as an energy filter to perform cooling using a potential bias. Figure is taken from [121]. (b) Sketch of a QD-based heat engine with a single energy level. The QD is coupled to hot and cold reservoirs. An electron traverses the QD energy level and converts part of its heat into useful work. By applying a higher voltage to the cold reservoir and tuning the energy level of the QD, the setup can act as a refrigerator, transferring heat out of the cold reservoir. Figure is taken from [122].

heat engine to generate power [23, 24, 118], but more relevant here in this thesis, as a refrigerator, meaning it can be used to transfer heat out of a cold reservoir by using a potential bias, Fig. (5.1). Particularly for QPCs, enhanced thermoelectric cooling has been experimentally proven [119]. QPC is favorable for large output powers and sizable efficiencies of a given output power [120].

Another type of energy filtering is given by QDs. QDs are good models to study thermoelectric effects [123–126]. There have been recent experimental investigations on thermoelectric properties of QDs [122, 127], and particularly thermoelectric cooling in QDs [128]. The energy levels of a QD are tunable via external gates. A peculiar feature of QDs is the narrow energy window that its transmission probability provides. This makes the charge current passing through it and, therefore, the electrical power to be small. Since the peaked-shape transmission of a QD, described in chapter 4, provides a precise filtering of energy, ideal efficiencies that are close to Carnot efficiency can, in principle, be reached in a QD refrigerator in the linear-response regime [129–131]. This high efficiency is because of the small absorbed power required for the cooling process that is a result of the distinct energy filtering of QD. Achieving high efficiencies results in promising applications of QDs for cooling. However, due to the small width of the energy level, QD devices can typically not produce considerable output power

Unlike the straight forward energy filtering model of QPC and QD, a quantum spin Hall (QSH) device with a magnetic island, as described in chapter 4 provides more complex features in its energy-dependent transmission. The performance of setups based on the QSH device has been studied, working as a quantum heat

engine and a refrigerator [132, 133]. These operations have been studied mainly in the linear response regime. The linear response regime works for small temperature and voltage differences. In a recent work, thermoelectric properties are studied in the QSH device, in which QSH edge states are coupled to a nanomagnet [26]. In chapter 4 the transmission probability of this QSH device containing a magnetic island is described. This transmission shows rapid oscillations with energy resulting from the backscattering of edge states from the magnetic island.

As shown in chapter 4, the QSH transmission shows energy filtering properties that in different limits are similar to the ones in QPC and QD transmissions. This motivates the analysis of the thermoelectric performance of the complicated energy filtering in the QSH transmission by taking advantage of these similarities in different limits. In paper II we use these similarities to analyze the thermoelectric cooling performance of the QSH device with a magnetic island. We provide analyses of the operation of the device beyond linear response regimes.

It is worth noting that due to the quantum effects, there is an upper limit to the heat energy that can be transferred and the power that can be produced in mesoscopic devices. Here, in the next section, we discuss these limits.

5.1.1 Pendry's quantum bound

Quantum mechanics imposes bounds on quantities such as the power produced and heat current transferred in mesoscopic systems. These bounds were first derived by Pendry [134] using Landauer scattering theory. For the rate of heat flow, there is an upper bound on the heat flowing out of a reservoir with a temperature T through a quantum system. This bound is attained when all the particles arriving at the quantum system in each mode transmit through the barrier. This quantum bound is [24, 135]

$$J_{\text{qb}} = \frac{\pi^2 N k_{\text{B}}^2}{6h} T^2, \quad (5.2)$$

where N is the number of modes. This quantum bound has been experimentally observed in QPCs and quantum Hall edge-states [136, 137]. It is shown in [135] that the upper bound on the cooling power of any refrigerator is half of the Pendry quantum bound for heat current, $J_{\text{qb}}/2$. Our results in paper II obeys this bound on cooling power.

The quantum bound also applies to the power produced in heat engines. In Refs. [24, 135, 138], considering maximums of heat flow and efficiency, which is

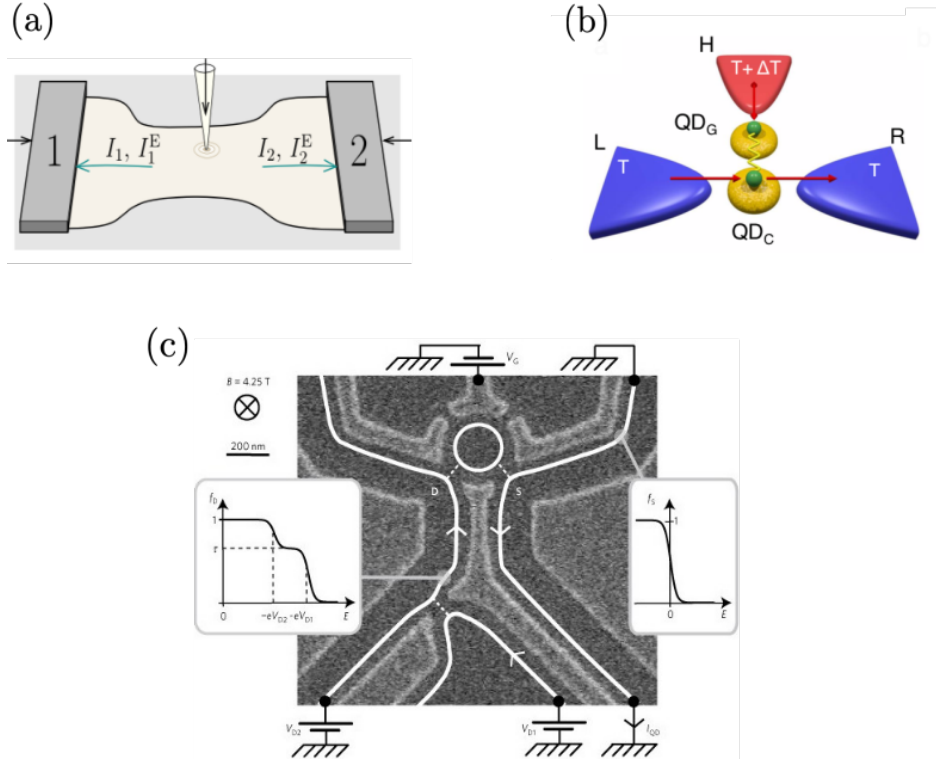


Figure 5.2: (a) Sketch of a working system into which an input flow is injected. Figure is taken from [31]. (b) Schematic of a three-terminal device with one hot reservoir (red) that can exchange electrons (green) with a quantum dot (yellow disc). The working system is the other two reservoirs (L and R, blue) that are at a lower temperature. The hot reservoir transfers heat to the working system via Coulomb interaction (yellow wave) between electrons in quantum dots. Figure is taken from [140]. (c) Sketch of the sample that is used to detect a nonequilibrium distribution. The brighter color shows the metallic gates and the edge channels are shown by solid white lines. White dashed lines show the partly transmission of edge channels across the QPC and QD. The QPC is used to drive the edge channels out-of-equilibrium. The left and right insets show nonequilibrium and equilibrium electron distributions respectively. Figure is taken from [141]

the Carnot efficiency, an upper bound for the generated power in heat engines is found. This bound that we here call Whitney power, in a system with hot and cold baths with temperatures T_{hot} and T_{cold} is

$$P_w = \frac{A_0 \pi^2 k_B^2}{h} (T_{\text{hot}} - T_{\text{cold}})^2, \quad (5.3)$$

where $A_0 \simeq 0.0321$. The bound on power has also been tested in a recent experiment [139]. We use both the quantum bound on heat flow and Whitney power in paper III.

5.2 Nonequilibrium resource

Generally, a thermodynamic system exploits a resource in order to perform a certain process. This input is usually a flow of energy, heat, work, or power from a source that can be separated from the working system, panel (a) of Fig. (5.2). This can be thought of as a multi-terminal device with one terminal injecting a resource to the rest of the device that acts as the working system. A schematic of an example for an electronic three-terminal device based on quantum dots is shown in panel (b) of Fig.(5.2), where a hot bath transfers heat into the working system via Coulomb interaction [140]. The bath considered in this example is in thermal equilibrium. However, the input to the working system can be from a non-thermal bath that is not in thermal equilibrium [142–144].

Typically, the scales in nanostructures are much smaller than the thermalization length of electrons. This means that electrons can have a far from equilibrium distribution, and the impact of this distribution should be considered in describing nanoscale systems. The nonequilibrium distribution can be produced in various experimental configurations. One of these experiments was employed in a multi-terminal setup containing normal and superconductors [145]. This setup is based on SNS Josephson junctions with extra leads connecting the normal part to a sizeable normal reservoir. This experiment is performed in the diffusive limit where the electron mean free path is much shorter than the sample length and the phase coherence length. In this experiment, the two superconductors are kept at the same potential. A nonequilibrium distribution is produced by applying different potentials to the normal reservoir to make the electronic distribution deviate from equilibrium. Shortly after this, in another experiment, distributions out of equilibrium have been experimentally detected for edge channels [141]; see panel (c) of Fig. (5.2). In this experiment, the resulting distribution is measured from a tunnel current through a quantum dot placed at a short distance from the QPC. Such distributions that are out of equilibrium can be used as inputs to a working system. In this case, it is shown that even in the absence of heat or power flow into the working system, it is possible to produce power or perform cooling by exploiting the nonequilibrium distribution [31]. In the same line as this work, in paper III, we propose a multi-terminal setup in a quantum Hall system and investigate the influence of a nonequilibrium distribution as a resource, in addition to power or energy flows, on the operation of a working system.

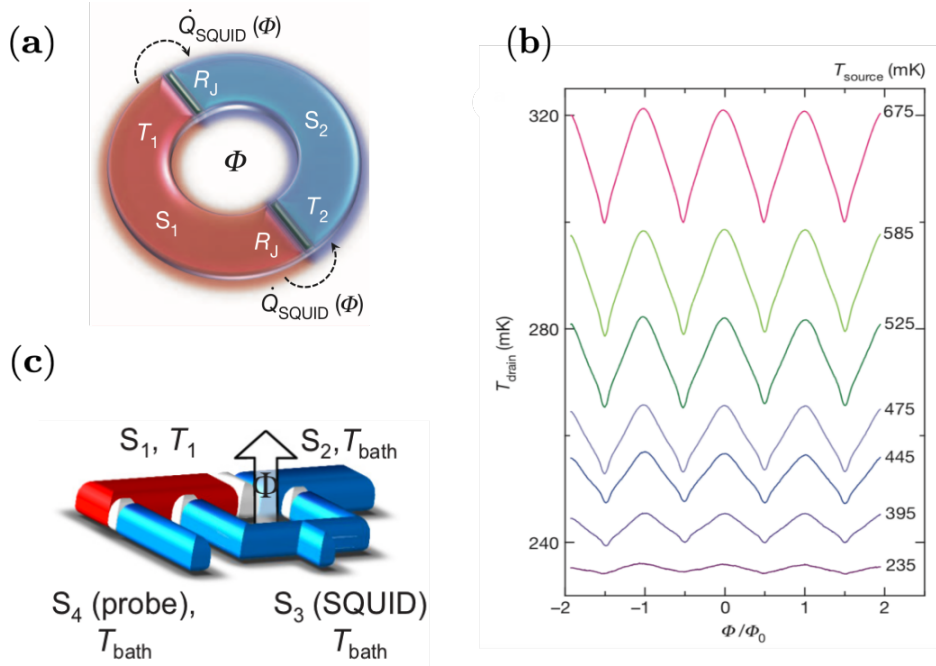


Figure 5.3: (a) Scheme of a temperature biased SQUID made of two identical superconductors S_1 and S_2 . Temperature T_1 is kept fixed, while the temperature $T_2 < T_1$ is influenced by the heat flow across the junctions. R_J is the normal state resistance of each junction and $\dot{Q}_{\text{SQUID}}(\Phi)$ is the heat current flowing from the hotter to the colder superconductor. (b) Flux modulation of the drain temperature $T_{\text{drain}} \equiv T_2$ of the superconductor S_2 in the structure shown in (a). Figures are taken from [36]. (c) Phase-biasing a Josephson junction by means of a three-junction SQUID. Figure is taken from [146].

5.3 Phase-dependent heat transport

The superconducting phase provides a new parameter that can be used to control and regulate heat transport in superconducting devices. This leads to the development of phase-coherent caloritronics. It was predicted theoretically in 1965 that heat currents through Josephson junctions depend on the relative phase difference between the superconductors [32]. This dependence is shown in the tunneling regime as

$$J = \frac{1}{h} \sum_{n=0}^{\mathcal{N}} \int_0^{\infty} dE E D_n \left(\frac{E^2 - \Delta_L \Delta_R \cos \varphi}{\sqrt{E^2 - \Delta_L^2} \sqrt{E^2 - \Delta_R^2}} \right) [f_L(E) - f_R(E)], \quad (5.4)$$

where we see the dependence of heat current (J) on phase (φ) is through the transmission probability. This shows by controlling this phase, the heat current can be controlled.

For the first time, the phase-dependence of the quasiparticle heat currents

in superconductors was proved in an experiment for heat transport across a Josephson junction [36]. Josephson junctions form the basis of an extensively used device, the superconducting quantum interference device (SQUID) [98] that is also used in this first experimental realization. In panels (a) and (b) of Fig. (5.3) a schematic sketch of the setup and the results of this realization are shown. The basic ingredient of the experiment is a SQUID, which allows for a modulation of the superconducting phase-difference via an applied magnetic flux. One of the SQUID segments is heated to a fixed temperature T_1 . The quasiparticle heat flow across the junction results in a measurable temperature change on the other side of the junction, T_2 . Due to the phase-dependence of the heat current, the resulting temperature change is phase-dependent. This can be seen in panel (b) of Fig. (5.3). Subsequently, the phase-dependent control of heat currents has been the basis for a number of experimental proposals [37]. In these experiments, by biasing different phases in similar setups as stated above, the amount of heat flowing in different directions can be controlled, resulting in the experimental design of a heat diode and different configurations of thermal transistors, which might operate as a thermal switch or as an amplifier/modulator [37]. These designs are based on a three-junction SQUID, shown in panel (c) of Fig. (5.3), in which a magnetic flux is used to apply a phase bias. These structures offer the thermal counterparts of electronic devices that can be used in thermal circuits and phase-coherent caloritronics.

More complicated structures such as multi-terminal devices are also of interest in phase-coherent caloritronics. In these devices, several superconducting phase differences provide a larger number of parameters to control heat. One example is three-terminal Josephson junction that can be used to realize heat circulators [40].

With the motivation arising from these studies, in paper I, we identify how the properties of hybrid superconducting junctions can influence the phase-coherent heat transport. We consider a disordered diffusive junction and analyze its impact on the phase-dependency of different heat transport quantities. Furthermore, in paper IV, we consider a three-terminal device with normal or superconducting contacts and analyze the influence of phase and magnetic field penetrating the setup on its performance as a heat circulator.

6 Overview of the appended papers

This chapter summarizes the motivation, approach, and findings of papers I-IV that constitute the research of this thesis. It should be noted that in all papers we use the Landauer-Büttiker scattering theory, as introduced in chapter 4, for our analyses.

6.1 Paper I

This paper provides an analysis of heat transport in superconducting and normal-metal hybrid structures. We considered the following systems: A Josephson junction, namely a superconductor-normal conductor-superconductor (SNS) across which a temperature- and a phase bias is applied. Also the gaps can be different. Furthermore, we study an NS junction, which corresponds to the previous case where one of the superconducting contacts has a vanishing gap. We analyze the linear-response heat conductance. The specific question we address here is how the properties of the disorder in the junction influence the phase- and gap-dependence of the heat conductance in SNS and NS hybrid junctions.

We analyze the heat transport in the SNS junction, in the single and multi-channel regimes. Following the approach in Ref. [147], we wrote the scattering matrix of the whole SNS junction in terms of the transmission eigenvalues D_n of the normal-conducting disordered region. This approach is beneficial since we can directly employ the statistical distribution of the disordered normal region's transmission eigenvalues to get a channel-average of the full SNS structure's heat conductance. For this, we use the Dorokhov distribution that is a previously obtained distribution function for disordered junctions from random-matrix theory. The obtained scattering matrix serves for the analysis of both types of structures, SNS and NS, which we are interested in. In the remainder of the paper, we use the obtained matrix to calculate the linear response heat conductance.

First, we consider a single-channel junction, showing that the heat conductance can, depending on gap ratio and phase differences, be larger than the heat conductance in normal conducting junctions.

In contrast, the disordered region of the junction, which we consider here, is characterized by a large number of transport channels. Therefore, we consider

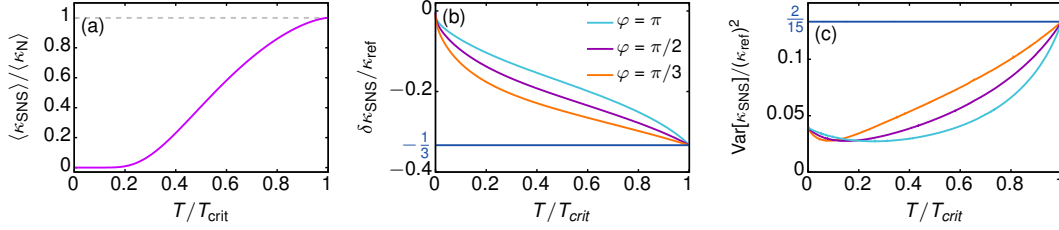


Figure 6.1: (a) The average heat conductance that is gap-ratio and phase independent. (b) Weak localization correction to the heat conductance at equal superconducting gaps at different phase differences. (c) Heat conductance fluctuations at equal superconducting gaps at different phase differences. The horizontal blue lines in panels (b) and (c) correspond to $\varphi = 0$. Figures are taken from the results of paper I [148].

the channel-averaged heat conductance, which is independent of the superconducting phases and gap ratio and only governed by temperature compared to the largest of the superconducting gaps in the structure, see panel (a) of Fig. (6.1).

Most importantly, we could identify an up-to-date unknown, non-trivial dependence of different quantities on the superconducting phase in SNS junctions. Namely, we find that in the weak localization correction to the average heat conductance, that is independent of the number of transport channels, the dependence on the superconducting phase difference is restored, panel (b) of Fig. (6.1).

Besides, our study addresses the heat conductance fluctuations. Importantly, our results show the persistence of the effects of phase difference and gap on this quantity, see panel (c) of Fig. (6.1). Regardless of the elaborated phase and gap dependence in heat conductance fluctuations, our results show that the heat conductance fluctuations have a close to universal behavior, similar to the well-known charge conductance fluctuations (fluctuations are of order unity compared to the (heat) conductance average). These fluctuations are independent of the junction length.

6.2 Paper II

The main goal of this work is to investigate a device in the quantum spin Hall (QSH) regime as a thermoelectric refrigerator. We analyze the cooling performance of such a device in a two-terminal setup both in the linear and in the nonlinear operation regimes with respect to temperature and voltage gradients.

The QSH device has a complex energy-dependent transmission which motivates the analysis of this setup as a thermoelectric cooling device. A vital feature of this transmission probability is that it has an energy gap with smooth boundaries. This results in similarities with a QPC device with a smooth step-like transmission. Another important feature of the QSH transmission are oscillations outside the gap, which are similar to resonance features in the transmission of quantum dots. These similarities motivate us to study the cooling performance of the QSH device by first investigating the cooling performance of a QPC and a quantum dot device and then use our results to analyze the QSH refrigerator. The results of this study are hence useful for different realistic devices.

We theoretically analyze the cooling power, namely the heat current flowing out of the cold reservoir. Besides the cooling power, the efficiency of the refrigerator known as the coefficient of performance is an important quantity to characterize the performance of the refrigerator, which we address in this paper. We present both analytical results for the step-like and resonant transmissions as well as a broad numerical analysis.

Indeed, analyzing the cooling performance of the QSH device, in different parameter ranges, we observe features similar to QPC and quantum dot devices with step-type and Lorentzian transmissions respectively, see Fig. (6.2). The results lead to the conclusion that the QSH device is comparable to a quantum dot device in low temperature regimes, panel (d) of Fig. (6.2). For higher temperature regimes, the QSH device's performance demonstrates a resemblance to the QPC model with high cooling power, panel (f) of Fig. (6.2).

Based on these observations, we identify optimal parameters for the device performance. As a starting point, we have discussed the range of parameters (electrochemical potential and temperature of the cold reservoir) for which cooling in a device with simplified well-shaped transmission, and hence similarly in a QSH device, is possible. From the result of cooling power for the well-shaped transmission, we showed that the electrochemical potential of the cold reservoir should probably be in the vicinity of one of the edges of the well, so that the evacuation of excitations from the cold contact exceeds the flow of excitation in the opposite direction. This is an essential requirement for optimizing cooling power.

At each edge of the well, the transmission has a step-like behavior. We investigate the influence of the smoothness of this step on the cooling performance. Our results show that for a sharp step, the maximum cooling power is achieved when the cold reservoir's electrochemical potential is at the edge of transmission

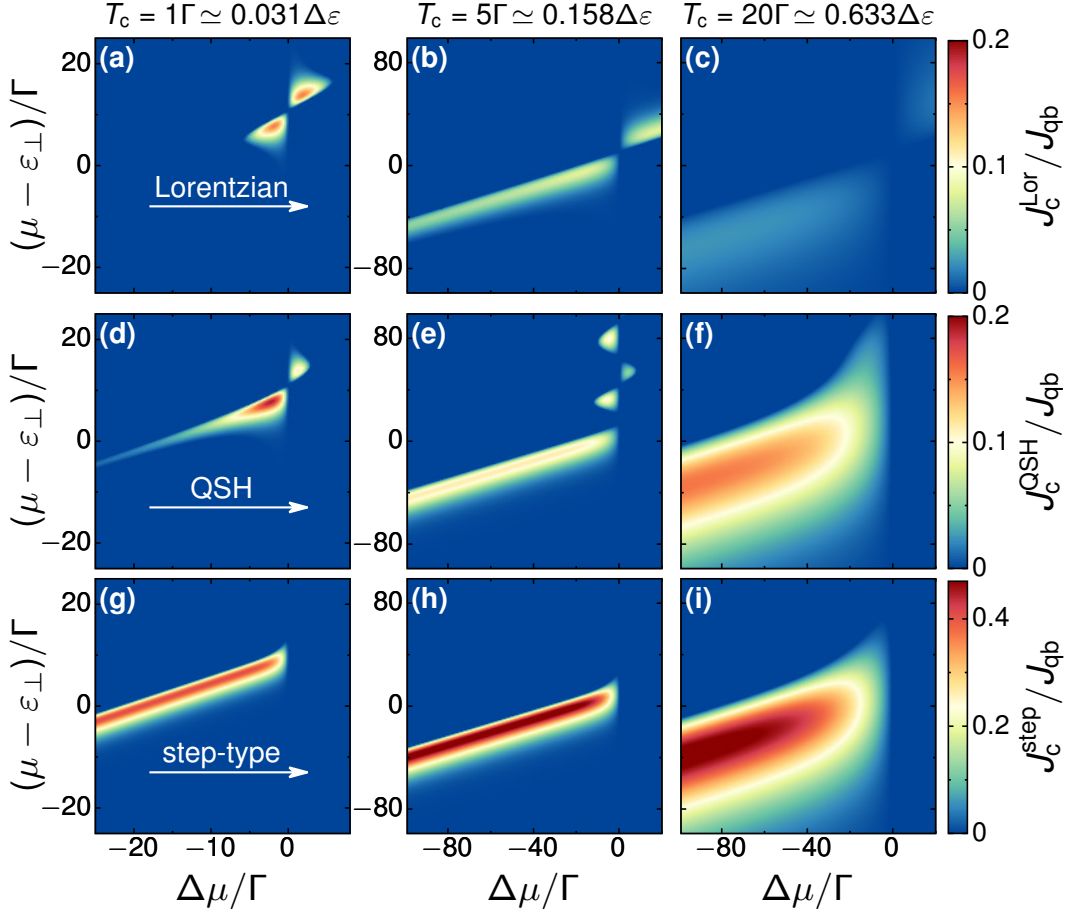


Figure 6.2: Cooling power of (a)-(c) a conductor described by a Lorentzian transmission function, (d)-(f) a QSH device, and (g)-(i) a conductor described by a step-type transmission function. Figures are taken from paper II [149].

function. We also identify the ideal point of cooling power for a smooth transmission. The results then provide the regions where substantial values for both cooling power and COP are achieved.

To address the influence of oscillations in the transmission of the QSH device, we discuss the cooling performance of a quantum dot device. In this limit, we find small cooling power, but high efficiencies that can be reached in the linear response regime.

The analysis of optimizations helps us to figure out in which parameter regimes the step-type or the Lorentzian transmissions play role. The key findings emerging from optimizations show that the cooling power can reach the quantum bound when the transmission is in the step position, and to get the maximum values of cooling power in low temperatures, we require small potential biases (linear regime). Besides, analyses of optimization for peaked transmission con-

firm available cooling for a broad range of parameters (such as voltage biases) in different regimes, leading to a double peak shape of cooling power. Regarding the efficiency, maximum COP happens in smaller voltage biases compared to the cooling power.

As shown in Fig. (6.2), in the QSH device, for higher temperatures, the dominating features of the cooling power is comparable to the step-type transmission of QPC model. In these temperature regimes, larger potential biases are required to achieve optimal cooling power (nonlinear regime). This shows the importance of the study in the nonlinear regime.

6.3 Paper III

This paper investigates the thermodynamic operation of a device exploiting a nonequilibrium distribution as a resource. The surprising feature in this device is that it can perform a thermodynamic process without absorbing heat or power. This feature is hence comparable to a demon! This is investigated in a previous study [31]. In this study, the device was called N-demon, with N indicating nonequilibrium. Here, we add crucial insights to the performance of this device, namely the influence of a nonequilibrium resource on the device's performance in the presence of heat flow to the working substance.

The setup we studied contains four terminals, of which two terminals (terminals 3 and 4 in Fig. (6.3)) are used to create the nonequilibrium in the resource region. This choice was employed because it makes controlling the nonequilibrium flow easier in experiment, and also, the calculation of entropy production in the resource region that we use in the paper is straightforward. Note, however, that any type of nonequilibrium distribution would be suitable. We choose a setup exposed to a perpendicular magnetic field (quantum Hall regime), where the charge and energy transport occur along chiral edge states. We use scatterers in both resource and working substance, next to terminals 4 and 1, as indicated in the Fig. (6.3)), for which we consider a QPC or a quantum dot.

We analyze the setup performing in analogy to different machines, including a heat engine to produce power, a standard refrigerator, and an absorption refrigerator that does cooling by heating. We investigate these machines' performance by analyzing the produced power in the heat engine, the cooling power of refrigerators, and, importantly, appropriate efficiencies.

We start by analyzing the plots of the produced power and heat currents

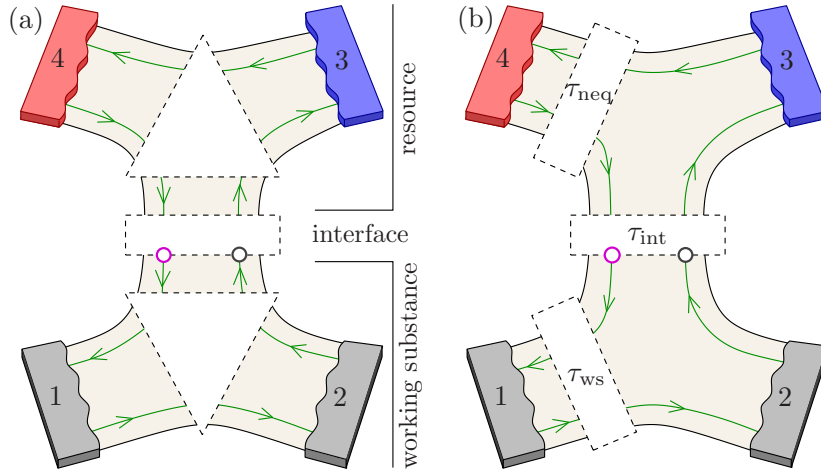


Figure 6.3: Injection of a nonequilibrium distribution into a working substance via quantum Hall edge states. The working substance includes terminals 1 and 2, and the nonequilibrium resource region includes terminals 3 and 4, and there is an interface between these two regions. Each of the regions contains a scattering region (white areas) with transmissions τ_{ws} , τ_{neq} and τ_{int} . The figure is taken from paper III [150].

flowing out of the resource region and the working substance. We specifically investigate how efficiencies behave in the three thermodynamic devices; heat engines, standard refrigerators, and absorption refrigerators. We first consider the conventional efficiency, which is a dimensionless ratio of the device's desired output (produced power in heat engine and cooling power in refrigerators) to the energy or heat currents from the resource region. Knowing from the laws of thermodynamics, the upper bound of these efficiencies are Carnot limits. Comparing the efficiencies to this limit, our results show that the conventional efficiencies exceed the Carnot limits. In addition to this, the conventional efficiencies diverge when there is zero energy or power flow from the resource region into the working substance. This shows that defining efficiencies here is tricky. The key point is that the influence of the nonequilibrium distribution is totally ignored in the definition of the conventional efficiencies.

Furthermore, we investigate another quantity that is based on entropy. It compares the entropy reduction in the working substance to the demon's entropy production, giving a good insight into the entropy balance in the system. This is called the entropy coefficient in the paper. When the flow of heat and power from the resource region is zero, this coefficient is always positive. However, this measure does not involve the produced power, therefore it is not a good measure of the full performance of the device.

As a well-behaved efficiency that considers both demonic and conventional

thermodynamic operations, and characterizes the device properly, we propose an efficiency based on the free energy of the nonequilibrium resource. This efficiency has upper bounds given by the laws of thermodynamics. This efficiency is adequate to describe the performance of the considered device since it includes all resources consumed for the device's performance. Our findings highlight that the free energy efficiencies are positive for the whole region of positive power produced or cooling power and give the desired information for the devices' characterization. We use this free energy efficiency further to describe the device's behavior as a heat engine with different combinations of QPC and quantum dot for scatterers considered in the setup.

Finally, in order to prove that it is the nonequilibrium resource that is the reason for the observed demonic effects, we show the suppression of the demonic action under the destruction of nonequilibrium distribution by thermalizing via a voltage and temperature probe.

6.4 Paper IV

In paper I, we saw the important impact of disorder for coherent heat transport. Here, we analyze realistic device conditions with parameters varying from sample to sample for a more complex device, namely a heat circulator. For this, in paper IV, we consider a three-terminal device with normal- or superconducting terminals, performing as a heat-current circulator.

A heat circulator is a device that provides a tunable control on heat flows and circulates heat in a preferred direction. In the considered setup in paper IV, the heat circulation can be controlled by imposing a superconducting phase bias between the terminals and more relevant here, by tuning a magnetic flux penetrating the junction area. We start analyzing the device's operation by addressing the comparison of heat circulation in devices with normal and superconducting contacts. First, an ideal ring-structure containing three sites is considered, and then a detailed study on conductors deviating from the ideal ring-structure with more than three sites is conducted. An important consequence of this is that the enclosed magnetic flux varies with each trajectory that a particle can follow between the contacts.

Starting from the ideal setup, our results demonstrate that in the ideal ring-structure configuration, under some circumstances, the heat circulation in a device with normal conducting contacts is more effective than the superconducting counterpart. We find that even for the parameters where the superconducting

circulator has a better performance than the normal one, the conductance in the normal setup is typically larger. It is worth noting that unlike in a previous study on a similar heat circulator [40], we here consider self-consistently the temperature-dependence of the superconducting gap.

Furthermore, we calculate the ensemble average of heat circulation over system parameters including on-site energies and hopping amplitudes between the sites, and also the variance of the heat circulation. For the ideal ring-structure model, we find that the circulation parameter does not fluctuate much around its ensemble-average. Our results reveal a reduction of just 15 percent of the circulation under random variation of system parameters. For more complicated non-ideal setups, we found that they are much more sensitive to fluctuations of the mentioned system parameters. However, for these structures high circulation can be achieved by properly tuning parameters.

In addition to this, we address structures for which the trajectory of particles in the scattering region is fully chaotic. Even though here the average circulation is fully suppressed, specific realizations still do good circulation for fixed parameters.

7 Summary

The study of heat transport and thermal effects in mesoscopic systems is the main focus of this thesis and its appended papers. We have shown how size confinement and quantum effects influence the transport of heat in mesoscopic scales.

Our specific interest has been the control and exploitation of heat transport by three specific properties of quantum systems: phase-coherence in superconducting junctions, energy filtering resulting from quantum confinement, and nonequilibrium distribution of resource contacts. We have studied how these properties can be exploited to control heat. We have analyzed and discussed heat transport in setups containing nanoscale elements and systems such as quantum Hall and quantum spin Hall edge states, quantum point contact and quantum dot, and superconducting hybrid junctions. These nanostructures and their properties were introduced in chapter 3. In order to analyze the heat transport in the considered systems, we have used the scattering theory that is introduced in chapter 4. Furthermore, in chapter 5 we reviewed some previous theoretical and experimental works on detection of the influence of mentioned effects on mesoscopic systems containing the nanoscale elements introduced in chapter 3.

This chapter summarizes the main contributions of this thesis to the topic of heat control. In paper I, we have specifically investigated phase-coherent heat transport in a Josephson junction containing a normal disordered scattering region between two superconductors. We analyze the behavior of thermal properties such as the linear-response heat conductance and, in particular the influence, which the junction properties have on heat transport. We find the average heat conductance over a large number of transport channels in the disordered junction using the previously obtained distribution functions for disordered junctions from random-matrix theory. Interestingly, this average turns out to be independent of the superconducting phase and differences between gaps. In addition, we address the weak localization correction to the heat conductance and the heat conductance fluctuations. Unlike the average of heat conductance, here, we identify an up-to-date unknown dependence on the superconducting phase and gap differences in SNS junctions. Importantly, we find these heat conductance fluctuations have a similarly universal behavior as the well-known charge con-

ductance fluctuations. This study motivated the investigation of phase-coherent heat transport in multi-terminal devices, which is the focus of paper IV.

In paper II, we studied thermoelectric cooling, which can be realized using the energy-filtering properties of a size-confined quantum conductor. The main device of interest is a quantum spin Hall conductor in which energy-dependent backscattering is induced by a magnetic island. Our predictions are based on a detailed analysis of fundamental device elements such as QPCs and QDs, separately showing the features occurring in the complex QSH transmission. These transmission probabilities have also been discussed in chapter 4. We have analyzed in detail the cooling power and coefficient of performance of the studied device in both linear and nonlinear regimes. Furthermore, we have presented experimentally accessible ranges of physically related parameters for which the cooling performance is optimum. The contributions made in this paper should be of wide interest to experimentalists exploring thermoelectric heat transport in systems with energy-filtering barriers.

The scope of paper III is the use of nonequilibrium effects for heat control and power production. We have considered a multi-terminal device where part of it acts as a nonequilibrium resource that drives the rest of the system, which takes the role of a working substance. A significant feature of this setup is that for the working substance to produce power or perform cooling, no heat flow from the resource region is required. We have presented a detailed analysis of the system's thermodynamic operation, including output powers and efficiencies of the device with different implementations. We observed that conventional efficiencies do not characterize the influence of the nonequilibrium resource. Therefore we investigated efficiencies based on free energies that reveal the key characteristics arising from the nonequilibrium resource.

Coming back to the phase-coherent heat transport in paper IV, we study a three-terminal setup containing normal- or superconducting contacts realizing a heat circulator. The device is penetrated by a magnetic flux. Exploiting the magnetic field as well as the superconducting phase to control heat circulation has been discussed in this paper. While superconducting devices have an additional tunability due to the phase, we find that normal conducting devices have typically a better performance as circulators. In addition to an ideal three-site ring structure, we analyze experimentally relevant non-ideal devices with more sites. Consequently, in these non-ideal rings the enclosed flux varies. We investigate the impacts of fluctuating hopping between the sites and on-site energies on heat circulation. As an extreme case of this, we analyze a chaotic cavity. While all more complex devices can act as circulators, we show that the detrimental effects of fluctuating parameters increase with the device complexity.

7.1 Outlook

To conclude, we briefly discuss possible future directions of research arising from this work.

In the context of heat control, another relevant quantity to study is higher-order correlation functions and noise for which we have already started the first analyses. As a further step in our research, it would be interesting to compute the heat current noise (the second-order correlation function between heat currents) to investigate how these fluctuations are affected by quantum effects in the systems we studied.

This noise study is of interest in all three contexts that we have addressed. In phase-coherent caloritronics further studies on heat current noise [151] might be addressed in future studies. In thermoelectric devices, heat noise is relevant to characterize the performance. In systems with nonequilibrium resource, noise allows to further analyze the underlying mechanisms [152].

In the context of the work of this thesis, which is the study of electronic heat transport, one can also analyze the phononic heat transport. Phononic heat transport, in particular in applications related to cooling, is expected to be of relevance. Also here, it can be important to compare the order of magnitude of effects calculated in this thesis to effects of phonon scatterings and electron-phonon interactions in heat transport.

Appendices

Appendix A

Absorption refrigerator

In Fig. (6) of paper III, the operation of an absorption refrigerator is shown for when terminal 1 of the working substance is considered as the cold terminal. Here we see what happens if we consider terminal 2 (the second terminal of the two in the working substance) as the cold terminal and try to cool it. The results for the cooling power $J_c^{\text{abs}} = -J_2$ are shown in panels (a) and (c) of Fig. (A.1). Both cases where the nonequilibrium distribution is created by a potential bias, $\mu_3 \neq \mu_4$ (left column), or by a temperature bias, $T_3 \neq T_4$ (right column) are shown. Similar to the results shown in Fig. (6) of paper III, the COP and the

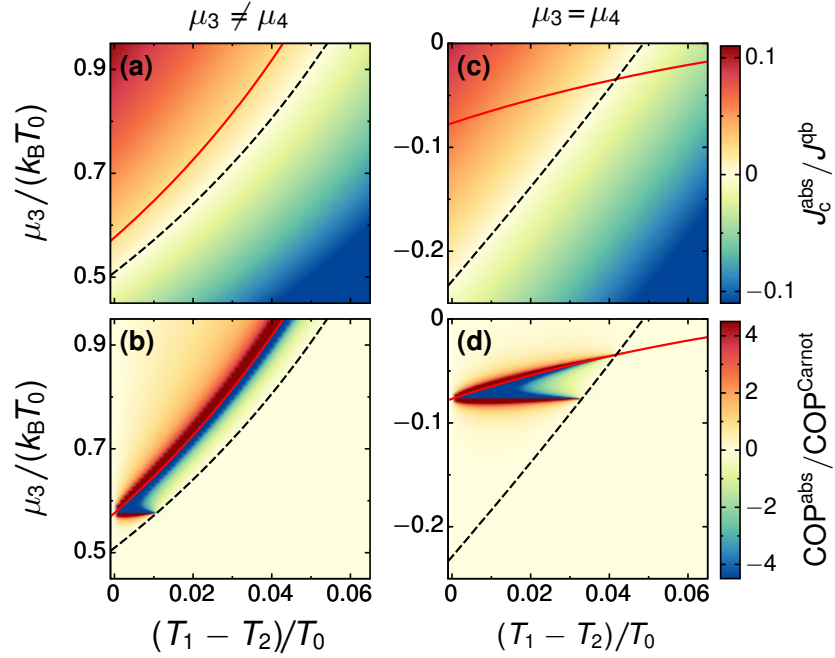


Figure A.1: Absorption refrigerator in the absence of charge currents from the resource region, $I_3 + I_4 = I_1 + I_2 \equiv 0$, and for $\mu_1 = \mu_2 = 0$ and $T_2 = T_0$. We take $E_{ws} = 0$ and fix E_{neq} by the condition of vanishing charge currents. In panels (a) and (b), we fix $T_3 = T_4 = 1.2T_0$ as well as $\mu_4/(k_B T_0) = -0.45$. In panels (c) and (d) we fix $T_3 = 0.9T_0$ and $T_4 = 1.2T_0$ as well as $\mu_4 = \mu_3$. At the full red line the additional condition $I_3^E + I_4^E = I_1^E + I_2^E \equiv 0$ is fulfilled. The black dashed line indicates where the cooling power is zero.

Carnot bound are defined as $\text{COP}^{\text{abs}} = \frac{J_c}{-I_3^E - I_4^E}$ and $\text{COP}^{\text{Carnot}} = \frac{1 - T_{\text{amb}}/T_{\text{hot}}}{T_{\text{amb}}/T_{\text{cold}} - 1}$ where $T_{\text{hot}} = T_{\text{p}}$. Here we have chosen to fix $T_2 = T_0$. We see a red region in the upper left part of panels (b) and (d) in Fig. (A.1). These regions show a real absorption refrigerator for which the cold terminal becomes colder. In the blue region of the same panels, we cool down contact 2 (the cold terminal), but heat up contact 1 in the working substance. In this region the resource has the ambient temperature. Then below the blue region, where there is another red region in the plot, both COP^{abs} and $\text{COP}^{\text{Carnot}}$ become negative and this makes the ration positive.

References

- [1] E. Scheer and J. C. Cuevas, *Molecular electronics: an introduction to theory and experiment*, Vol. 15 (World Scientific, 2017) (cit. on p. 1).
- [2] M. G. Pala and A. Cresti, “Increase of self-heating effects in nanodevices induced by surface roughness: A full-quantum study”, *J. Appl. Phys.* **117**, 084313 (2015) (cit. on p. 1).
- [3] F. Giazotto, T. T. Heikkilä, A. Luukanen, A. M. Savin, and J. P. Pekola, “Opportunities for mesoscopics in thermometry and refrigeration: Physics and applications”, *Rev. Mod. Phys.* **78**, 217–274 (2006) (cit. on pp. 1, 2, 4, 7).
- [4] O.-P. Saira, M. Meschke, F. Giazotto, A. M. Savin, M. Möttönen, and J. P. Pekola, “Heat Transistor: Demonstration of Gate-Controlled Electronic Refrigeration”, *Phys. Rev. Lett.* **99**, 027203 (2007) (cit. on pp. 1, 8).
- [5] Y. Dubi and M. Di Ventra, “Colloquium: Heat flow and thermoelectricity in atomic and molecular junctions”, *Rev. Mod. Phys.* **83**, 131–155 (2011) (cit. on pp. 1, 2).
- [6] J.-P. Fleurial, “Thermoelectric power generation materials: Technology and application opportunities”, *JOM* **61**, 79–85 (2009) (cit. on p. 1).
- [7] J. S. Lim, R. López, and D. Sánchez, “Dynamic thermoelectric and heat transport in mesoscopic capacitors”, *Phys. Rev. B* **88**, 201304 (2013) (cit. on p. 1).
- [8] G. Kiršanskas, Q. Li, K. Flensberg, G. C. Solomon, and M. Leijnse, “Designing π -stacked molecular structures to control heat transport through molecular junctions”, *Appl. Phys. Lett.* **105**, 233102 (2014) (cit. on p. 1).
- [9] M. A. Nielsen and I. Chuang, *Quantum Computation and Quantum Information*, Vol. 70, 5 (American Association of Physics TeachersAAPT, 2002) (cit. on p. 1).
- [10] Y. Yan and J. A. Malen, “Periodic heating amplifies the efficiency of thermoelectric energy conversion”, *Energy Environ. Sci.* **6**, 1267–1273 (2013) (cit. on p. 1).
- [11] A. Sood, F. Xiong, S. Chen, H. Wang, D. Selli, J. Zhang, C. J. McClellan, J. Sun, D. Donadio, Y. Cui, E. Pop, and K. E. Goodson, “An electrochemical thermal transistor”, *Nat. Commun.* **9**, 1–9 (2018) (cit. on p. 1).

-
- [12] A. Sood, E. Pop, M. Asheghi, and K. E. Goodson, “The Heat Conduction Renaissance”, 2018 17th IEEE Intersociety Conference on Thermal and Thermomechanical Phenomena in Electronic Systems (ITherm), 1396–1402 (2018) (cit. on p. 1).
 - [13] S. Juergens, F. Haupt, M. Moskalets, and J. Splettstoesser, “Thermoelectric performance of a driven double quantum dot”, *Phys. Rev. B* **87**, 245423 (2013) (cit. on p. 2).
 - [14] D. Venturelli, R. Fazio, and V. Giovannetti, “Minimal Self-Contained Quantum Refrigeration Machine Based on Four Quantum Dots”, *Phys. Rev. Lett.* **110**, 256801 (2013) (cit. on p. 2).
 - [15] R. Uzdin, A. Levy, and R. Kosloff, “Equivalence of Quantum Heat Machines, and Quantum-Thermodynamic Signatures”, *Phys. Rev. X* **5**, 031044 (2015) (cit. on p. 2).
 - [16] D. Sánchez, R. Sánchez, R. López, and B. Sothmann, “Nonlinear chiral refrigerators”, *Phys. Rev. B* **99**, 245304 (2019) (cit. on p. 2).
 - [17] A. Majumdar, “Thermoelectricity in Semiconductor Nanostructures”, *Science* **303**, 777–778 (2004) (cit. on p. 2).
 - [18] G. J. Snyder and E. S. Toberer, “Complex thermoelectric materials”, *Nat. Mater.* **7**, 105 (2008) (cit. on p. 2).
 - [19] J. P. Pekola, A. Kutvonen, and T. Ala-Nissila, “Dissipated work and fluctuation relations for non-equilibrium single-electron transitions”, *J. Stat. Mech.: Theory Exp.* **2013**, P02033 (2013) (cit. on p. 2).
 - [20] J. V. Koski, V. F. Maisi, T. Sagawa, and J. P. Pekola, “Experimental Observation of the Role of Mutual Information in the Nonequilibrium Dynamics of a Maxwell Demon”, *Phys. Rev. Lett.* **113**, 030601 (2014) (cit. on p. 2).
 - [21] M. Campisi, J. Pekola, and R. Fazio, “Nonequilibrium fluctuations in quantum heat engines: theory, example, and possible solid state experiments”, *New J. Phys.* **17**, 035012 (2015) (cit. on p. 2).
 - [22] G. Rosselló, R. López, and G. Platero, “Chiral Maxwell demon in a quantum Hall system with a localized impurity”, *Phys. Rev. B* **96**, 075305 (2017) (cit. on p. 2).
 - [23] G. Benenti, G. Casati, K. Saito, and R. S. Whitney, “Fundamental aspects of steady-state conversion of heat to work at the nanoscale”, *Physics Reports* **694**, 1–124 (2017) (cit. on pp. 2, 52).
 - [24] R. S. Whitney, “Most efficient quantum thermoelectric at finite power output”, *Physical review letters* **112**, 130601 (2014) (cit. on pp. 2, 52, 53).

-
- [25] M. Josefsson, A. Svilans, A. M. Burke, E. A. Hoffmann, S. Fahlvik, C. Thelander, M. Leijnse, and H. Linke, “A quantum-dot heat engine operating close to the thermodynamic efficiency limits”, *Nature nanotechnology* **13**, 920–924 (2018) (cit. on p. 2).
- [26] D. Gresta, M. Real, and L. Arrachea, “Optimal Thermoelectricity with Quantum Spin Hall Edge States”, *Phys. Rev. Lett.* **123**, 186801 (2019) (cit. on pp. 2, 3, 43, 53).
- [27] J. W. Gibbs, *Scientific Papers: Thermodynamics*, Vol. 1 (Dover Publications, 1961) (cit. on p. 3).
- [28] K. Sekimoto, *Stochastic energetics*, Vol. 799 (Springer, 2010) (cit. on p. 3).
- [29] U. Seifert, “Stochastic thermodynamics, fluctuation theorems and molecular machines”, *Reports on progress in physics* **75**, 126001 (2012) (cit. on p. 3).
- [30] R. S. Whitney, R. Sánchez, F. Haupt, and J. Splettstoesser, “Thermoelectricity without absorbing energy from the heat sources”, *Physica E* **75**, 257–265 (2016) (cit. on pp. 3, 4).
- [31] R. Sánchez, J. Splettstoesser, and R. S. Whitney, “Nonequilibrium System as a Demon”, *Phys. Rev. Lett.* **123**, 216801 (2019) (cit. on pp. 3, 4, 54, 55, 63).
- [32] K. Maki and A. Griffin, “Entropy Transport Between Two Superconductors by Electron Tunneling”, *Phys. Rev. Lett.* **15**, 921–923 (1965) (cit. on pp. 4, 5, 29, 56).
- [33] J. T. Muhonen, M. Meschke, and J. P. Pekola, “Micrometre-scale refrigerators”, *Rep. Prog. Phys.* **75**, 046501 (2012) (cit. on pp. 4, 14).
- [34] M. J. Martínez-Pérez and F. Giazotto, “Efficient phase-tunable Josephson thermal rectifier”, *Appl. Phys. Lett.* **102**, 182602 (2013) (cit. on p. 4).
- [35] M. José Martínez-Pérez and F. Giazotto, “A quantum diffractor for thermal flux”, *Nat. Commun.* **5**, 3579 (2014) (cit. on pp. 4, 5).
- [36] F. Giazotto and M. J. Martínez-Pérez, “The Josephson heat interferometer”, *Nature* **492**, 401 (2012) (cit. on pp. 5, 28, 29, 56, 57).
- [37] A. Fornieri and F. Giazotto, “Towards phase-coherent caloritronics in superconducting circuits”, *Nat. Nanotechnol.* **12**, 944 (2017) (cit. on pp. 5, 57).
- [38] H. Q. Nguyen, T. Aref, V. J. Kauppila, M. Meschke, C. B. Winkelmann, H. Courtois, and J. P. Pekola, “Trapping hot quasi-particles in a high-power superconducting electronic cooler”, *New J. Phys.* **15**, 085013 (2013) (cit. on p. 5).

-
- [39] G. Viola and D. P. DiVincenzo, “Hall Effect Gytrators and Circulators”, *Phys. Rev. X* **4**, 021019 (2014) (cit. on pp. 5, 9).
- [40] S.-Y. Hwang, F. Giazotto, and B. Sothmann, “Phase-Coherent Heat Circulator Based on Multiterminal Josephson Junctions”, *Phys. Rev. Appl.* **10**, 044062 (2018) (cit. on pp. 5, 9, 47, 57, 66).
- [41] D. Kondepudi and I. Prigogine, “From heat engines to dissipative structures”, *Modern Thermodynamics*, John Wiley & Sons Chichester **25** (1998) (cit. on p. 8).
- [42] F. Giazotto and F. S. Bergeret, “Phase-tunable colossal magnetothermal resistance in ferromagnetic Josephson valves”, *Appl. Phys. Lett.* **102**, 132603 (2013) (cit. on p. 8).
- [43] A. Ronzani, B. Karimi, J. Senior, Y.-C. Chang, J. T. Peltonen, C. Chen, and J. P. Pekola, “Tunable photonic heat transport in a quantum heat valve”, *Nat. Phys.* **14**, 991–995 (2018) (cit. on p. 8).
- [44] C. L. Hogan, “The Ferromagnetic Faraday Effect at Microwave Frequencies and its Applications”, *Rev. Mod. Phys.* **25**, 253–262 (1953) (cit. on p. 9).
- [45] A. Nagulu, N. Reiskarimian, and H. Krishnaswamy, “Non-reciprocal electronics based on temporal modulation”, *Nat. Electron.* **3**, 241–250 (2020) (cit. on p. 9).
- [46] S. Bosco, F. Haupt, and D. P. DiVincenzo, “Self-impedance-matched Hall-effect gyrators and circulators”, *Physical Review Applied* **7**, 024030 (2017) (cit. on p. 9).
- [47] D. S. L. Cardwell, D. S. L. Cardwell, D. S. L. Cardwell, and D. S. L. Cardwell, *From Watt to Clausius: The rise of thermodynamics in the early industrial age* (Cornell University Press Ithaca, NY, 1971) (cit. on p. 9).
- [48] S. Carnot, “Reflections on the motive power of fire, and on machines fitted to develop that power”, Paris: Bachelier (1824) (cit. on p. 9).
- [49] G. J. Van Wylen, R. E. Sonntag, and C. Borgnakke, *Fundamentals of classical thermodynamics* (Wiley New York, 1976) (cit. on p. 10).
- [50] T. Seebeck, “Ueber die magnetische Polarisation der Metalle und Erze durch Temperaturdifferenz.[Magnetic polarization of metals and ores by temperature differences]”, *Abhandlungen der K. Akad. der Wissenschaften zu Berlin* **82**, 265–373 (1826) (cit. on p. 10).
- [51] J. Peltier, “New experiments on the heat effects of electric currents”, *Ann. Chim. Phys* **56**, 371–386 (1834) (cit. on p. 10).
- [52] G. Benenti, G. Casati, K. Saito, and R. S. Whitney, “Fundamental aspects of steady-state conversion of heat to work at the nanoscale”, *Phys. Rep.* **694**, 1–124 (2017) (cit. on pp. 11, 13–15).

-
- [53] J. P. Heremans, M. S. Dresselhaus, L. E. Bell, and D. T. Morelli, “When thermoelectrics reached the nanoscale”, *Nat. Nanotechnol.* **8**, 471–473 (2013) (cit. on p. 11).
- [54] J.-H. Jiang, O. Entin-Wohlman, and Y. Imry, “Thermoelectric three-terminal hopping transport through one-dimensional nanosystems”, *Phys. Rev. B* **85**, 075412 (2012) (cit. on p. 11).
- [55] L. Onsager, “Reciprocal Relations in Irreversible Processes. I.”, *Phys. Rev.* **37**, 405–426 (1931) (cit. on p. 11).
- [56] H. J. Goldsmid et al., *Introduction to thermoelectricity*, Vol. 121 (Springer, 2010) (cit. on p. 11).
- [57] M. Kardar, *Statistical physics of particles* (Cambridge University Press, 2007) (cit. on p. 12).
- [58] L. A. Correa, J. P. Palao, D. Alonso, and G. Adesso, “Quantum-enhanced absorption refrigerators”, *Sci. Rep.* **4**, 1–9 (2014) (cit. on p. 14).
- [59] P. A. Erdman, B. Bhandari, R. Fazio, J. P. Pekola, and F. Taddei, “Absorption refrigerators based on Coulomb-coupled single-electron systems”, *Phys. Rev. B* **98**, 045433 (2018) (cit. on p. 14).
- [60] T. Yamamoto, Yu. A. Pashkin, O. Astafiev, Y. Nakamura, and J. S. Tsai, “Demonstration of conditional gate operation using superconducting charge qubits”, *Nature* **425**, 941–944 (2003) (cit. on p. 17).
- [61] L. Trifunovic, O. Dial, M. Trif, J. R. Wootton, R. Abebe, A. Yacoby, and D. Loss, “Long-Distance Spin-Spin Coupling via Floating Gates”, *Phys. Rev. X* **2**, 011006 (2012) (cit. on p. 17).
- [62] M. D. Shulman, O. E. Dial, S. P. Harvey, H. Bluhm, V. Umansky, and A. Yacoby, “Demonstration of Entanglement of Electrostatically Coupled Singlet-Triplet Qubits”, *Science* **336**, 202–205 (2012) (cit. on p. 17).
- [63] L. Casparis, M. R. Connolly, M. Kjaergaard, N. J. Pearson, A. Kringhøj, T. W. Larsen, F. Kuemmeth, T. Wang, C. Thomas, S. Gronin, G. C. Gardner, M. J. Manfra, C. M. Marcus, and K. D. Petersson, “Superconducting gatemon qubit based on a proximitized two-dimensional electron gas”, *Nat. Nanotechnol.* **13**, 915–919 (2018) (cit. on p. 17).
- [64] S. Wu, L. Cheng, H. Yu, and Q. Wang, “Gate control of quantum dot-based electron spin-orbit qubits”, *Phys. Lett. A* **382**, 1922–1932 (2018) (cit. on p. 17).
- [65] J. P. Pekola, O.-P. Saira, V. F. Maisi, A. Kempainen, M. Möttönen, Y. A. Pashkin, and D. V. Averin, “Single-electron current sources: Toward a refined definition of the ampere”, *Rev. Mod. Phys.* **85**, 1421–1472 (2013) (cit. on p. 17).

-
- [66] S. J. Koester, K. Ismail, and J. O. Chu, “Determination of spin- and valley-split energy levels in strained Si quantum wells”, *Semicond. Sci. Technol.* **12**, 384–388 (1997) (cit. on p. 18).
- [67] S. Datta, *Electronic transport in mesoscopic systems* (Cambridge university press, 1997) (cit. on p. 18).
- [68] K. v. Klitzing, G. Dorda, and M. Pepper, “New Method for High-Accuracy Determination of the Fine-Structure Constant Based on Quantized Hall Resistance”, *Phys. Rev. Lett.* **45**, 494–497 (1980) (cit. on p. 19).
- [69] B. J. van Wees, L. Kouwenhoven, E. Willems, C. Harmans, J. Mooij, H Van Houten, C. Beenakker, J. Williamson, and C. Foxon, “Quantum ballistic and adiabatic electron transport studied with quantum point contacts”, *Physical Review B* **43**, 12431 (1991) (cit. on p. 19).
- [70] A. S. Dzurak, C. G. Smith, L. Martin-Moreno, M. Pepper, D. A. Ritchie, G. A. C. Jones, and D. G. Hasko, “Thermopower of a one-dimensional ballistic constriction in the non-linear regime”, *J. Phys.: Condens. Matter* **5**, 8055–8064 (1993) (cit. on p. 19).
- [71] R. Taboryski, A. Kristensen, C. B. So/rensen, and P. E. Lindelof, “Conductance-quantization broadening mechanisms in quantum point contacts”, *Phys. Rev. B* **51**, 2282–2286 (1995) (cit. on p. 19).
- [72] D. A. Wharam, T. J. Thornton, R. Newbury, M. Pepper, H. Ahmed, J. E. F. Frost, D. G. Hasko, D. C. Peacock, D. A. Ritchie, and G. A. C. Jones, “One-dimensional transport and the quantisation of the ballistic resistance”, *J. Phys. C: Solid State Phys.* **21**, L209–L214 (1988) (cit. on p. 20).
- [73] L. W. Molenkamp, H. van Houten, C. W. J. Beenakker, R. Eppenga, and C. T. Foxon, “Quantum oscillations in the transverse voltage of a channel in the nonlinear transport regime”, *Phys. Rev. Lett.* **65**, 1052–1055 (1990) (cit. on p. 20).
- [74] Y. V. Nazarov and Y. M. Blanter, *Quantum transport: introduction to nanoscience* (Cambridge University Press, 2009) (cit. on pp. 20, 31, 40, 47).
- [75] T. H. Oosterkamp, L. P. Kouwenhoven, A. E. A. Koolen, N. C. van der Vaart, and C. J. P. M. Harmans, “Photon Sidebands of the Ground State and First Excited State of a Quantum Dot”, *Phys. Rev. Lett.* **78**, 1536–1539 (1997) (cit. on p. 20).
- [76] M. A. Reed, J. N. Randall, R. J. Aggarwal, R. J. Matyi, T. M. Moore, and A. E. Wetsel, “Observation of discrete electronic states in a zero-dimensional semiconductor nanostructure”, *Phys. Rev. Lett.* **60**, 535–537 (1988) (cit. on p. 20).

-
- [77] L. P. Kouwenhoven, B. J. van Wees, K. J. P. M. Harmans, and J. G. Williamson, “Transport through zero-dimensional states in a quantum dot”, *Surf. Sci.* **229**, 290–297 (1990) (cit. on p. 20).
- [78] Y. Alhassid, “The statistical theory of quantum dots”, *Rev. Mod. Phys.* **72**, 895–968 (2000) (cit. on pp. 20, 21, 40).
- [79] C. W. J. Beenakker and A. A. M. Staring, “Theory of the thermopower of a quantum dot”, *Phys. Rev. B* **46**, 9667–9676 (1992) (cit. on p. 21).
- [80] A. A. M. Staring, L. W. Molenkamp, B. W. Alphenaar, H. van Houten, O. J. A. Buyk, M. A. A. Mabesoone, C. W. J. Beenakker, and C. T. Foxon, “Coulomb-Blockade Oscillations in the Thermopower of a Quantum Dot”, *EPL* **22**, 57–62 (1993) (cit. on p. 21).
- [81] A. G. Pogosov, M. V. Budantsev, R. A. Lavrov, A. E. Plotnikov, A. K. Bakarov, A. I. Toropov, and J. C. Portal, “Coulomb blockade and the thermopower of a suspended quantum dot”, *JETP Lett.* **83**, 122–126 (2006) (cit. on p. 21).
- [82] T. Ihn, *Semiconductor Nanostructures: Quantum states and electronic transport* (Oxford University Press, 2010) (cit. on p. 21).
- [83] L. P. Kouwenhoven, G. Schön, and L. L. Sohn, “Introduction to mesoscopic electron transport”, in *Mesoscopic electron transport* (Springer, 1997), pp. 1–44 (cit. on p. 21).
- [84] A. W. Holleitner, C. R. Decker, H. Qin, K. Eberl, and R. H. Blick, “Coherent Coupling of Two Quantum Dots Embedded in an Aharonov-Bohm Interferometer”, *Phys. Rev. Lett.* **87**, 256802 (2001) (cit. on p. 21).
- [85] A. Fuhrer, S. Lüscher, T. Ihn, T. Heinzel, K. Ensslin, W. Wegscheider, and M. Bichler, “Energy spectra of quantum rings”, *Nature* **413**, 822–825 (2001) (cit. on p. 21).
- [86] R. Leturcq, D. Sánchez, G. Götz, T. Ihn, K. Ensslin, D. C. Driscoll, and A. C. Gossard, “Magnetic Field Symmetry and Phase Rigidity of the Nonlinear Conductance in a Ring”, *Phys. Rev. Lett.* **96**, 126801 (2006) (cit. on p. 21).
- [87] T. Kuzmenko, K. Kikoin, and Y. Avishai, “Magnetically Tunable Kondo–Aharonov-Bohm Effect in a Triangular Quantum Dot”, *Phys. Rev. Lett.* **96**, 046601 (2006) (cit. on p. 21).
- [88] M. Sigrist, T. Ihn, K. Ensslin, M. Reinwald, and W. Wegscheider, “Coherent Probing of Excited Quantum Dot States in an Interferometer”, *Phys. Rev. Lett.* **98**, 036805 (2007) (cit. on p. 21).

- [89] M. Sigrist, T. Ihn, K. Ensslin, V. Puller, and Y. Meir, “Phase-coherent Electron Transport through Double Dots”, in *Perspectives of Mesoscopic Physics* (WORLD SCIENTIFIC, Singapore, 2010), pp. 305–315 (cit. on p. 21).
- [90] F. Borsoi, K. Zuo, S. Gazibegovic, R. L. M. O. het Veld, E. P. A. M. Bakkers, L. P. Kouwenhoven, and S. Heedt, “Transmission phase read-out of a large quantum dot in a nanowire interferometer”, *Nat. Commun.* **11**, 1–6 (2020) (cit. on p. 21).
- [91] E. H. Hall, “On a new action of the magnet on electric currents”, *Am. J. Sci. Series 3 Vol. 19*, 200–205 (1880) (cit. on p. 22).
- [92] B. J. van Wees, H. van Houten, C. W. J. Beenakker, J. G. Williamson, L. P. Kouwenhoven, D. van der Marel, and C. T. Foxon, “Quantized conductance of point contacts in a two-dimensional electron gas”, *Phys. Rev. Lett.* **60**, 848–850 (1988) (cit. on p. 22).
- [93] D. K. Ferry and S. Goodnick, *Transport in Nanostructures* (Cambridge University Press, 1997) (cit. on p. 23).
- [94] B. A. Bernevig, T. L. Hughes, and S.-C. Zhang, “Quantum Spin Hall Effect and Topological Phase Transition in HgTe Quantum Wells”, *Science* **314**, 1757–1761 (2006) (cit. on p. 24).
- [95] F. Dolcini, “Full electrical control of charge and spin conductance through interferometry of edge states in topological insulators”, *Phys. Rev. B* **83**, 165304 (2011) (cit. on p. 25).
- [96] P. Sternativo and F. Dolcini, “Effects of disorder on electron tunneling through helical edge states”, *Phys. Rev. B* **90**, 125135 (2014) (cit. on pp. 25, 44).
- [97] *Introduction to Superconductivity: Second Edition*, [Online; accessed 25. Oct. 2018] (2018) (cit. on pp. 27, 28).
- [98] J. Clarke and A. I. Braginski, *The SQUID Handbook* (2005) (cit. on pp. 28, 57).
- [99] B. D. Josephson, “Possible new effects in superconductive tunnelling”, *Physics Letters* **1**, 251–253 (1962) (cit. on p. 28).
- [100] B. D. Josephson, “The discovery of tunnelling supercurrents”, *Rev. Mod. Phys.* **46**, 251–254 (1974) (cit. on p. 28).
- [101] A. F. Andreev, “The thermal conductivity of the intermediate state in superconductors”, *JETP* **19**, [Online; accessed 13. Nov. 2018], 1228 (1964) (cit. on p. 29).
- [102] R. Landauer, “Spatial Variation of Currents and Fields Due to Localized Scatterers in Metallic Conduction”, *IBM J. Res. Dev.* **1**, 223–231 (1957) (cit. on pp. 31, 33).

-
- [103] R. Landauer, “Electrical resistance of disordered one-dimensional lattices”, *Philosophical Magazine: A Journal of Theoretical Experimental and Applied Physics* **21**, 863–867 (1970) (cit. on p. 31).
- [104] R. Landauer, “Electrical transport in open and closed systems”, *Z. Phys. B: Condens. Matter* **68**, 217–228 (1987) (cit. on p. 31).
- [105] M. Büttiker, “Four-Terminal Phase-Coherent Conductance”, *Phys. Rev. Lett.* **57**, 1761–1764 (1986) (cit. on pp. 31, 33).
- [106] M. Moskalets, *Scattering Matrix Approach to Non-Stationary Quantum Transport* (Imperial College Press, 2011) (cit. on p. 31).
- [107] P. N. Butcher, “Thermal and electrical transport formalism for electronic microstructures with many terminals”, *J. Phys.: Condens. Matter* **2**, 4869–4878 (1990) (cit. on p. 33).
- [108] R. De-Picciotto, M. Reznikov, M. Heiblum, V. Umansky, G. Bunin, and D. Mahalu, “Direct observation of a fractional charge”, *Physica B* **249-251**, 395–400 (1998) (cit. on p. 37).
- [109] M. Büttiker, “Scattering theory of current and intensity noise correlations in conductors and wave guides”, *Phys. Rev. B* **46**, 12485–12507 (1992) (cit. on p. 37).
- [110] Ya. M. Blanter and M. Büttiker, “Shot noise in mesoscopic conductors”, *Phys. Rep.* **336**, 1–166 (2000) (cit. on p. 37).
- [111] F. Hajiloo, *Phase dependent heat transport in superconducting junctions with scattering theory*. Thesis for the degree of Licentiate of Engineering. Technical report MC2: 405 (Department of Microtechnology and Nanoscience, Chalmers University of Technology, 2018) (cit. on pp. 39, 45).
- [112] A. D. Zaikin and D. Golubev, *Dissipative Quantum Mechanics of Nanostructures: Electron Transport, Fluctuations, and Interactions* (CRC Press, 2019) (cit. on pp. 40, 48).
- [113] R. A. Jalabert, A. D. Stone, and Y Alhassid, “Statistical theory of Coulomb blockade oscillations: Quantum chaos in quantum dots”, *Physical review letters* **68**, 3468 (1992) (cit. on p. 40).
- [114] M. Büttiker, “Quantized transmission of a saddle-point constriction”, *Phys. Rev. B* **41**, 7906–7909(R) (1990) (cit. on p. 42).
- [115] C. W. J. Beenakker, “Three “Universal” Mesoscopic Josephson Effects”, *SpringerLink*, 235–253 (1992) (cit. on p. 45).
- [116] J. S. Meyer and M. Houzet, “Nontrivial Chern Numbers in Three-Terminal Josephson Junctions”, *Phys. Rev. Lett.* **119**, 136807 (2017) (cit. on pp. 47, 48).

-
- [117] H. van Houten, L. W. Molenkamp, C. W. J. Beenakker, and C. T. Foxon, “Thermo-electric properties of quantum point contacts”, *Semicond. Sci. Technol.* **7**, B215–B221 (1992) (cit. on p. 51).
- [118] S. Kheradsoud, N. Dashti, M. Misiorny, P. P. Potts, J. Splettstoesser, and P. Samuelsson, “Power, Efficiency and Fluctuations in a Quantum Point Contact as Steady-State Thermoelectric Heat Engine”, *Entropy* **21**, 777 (2019) (cit. on p. 52).
- [119] U Ghoshal, S Ghoshal, C McDowell, L Shi, S Cordes, and M Farinelli, “Enhanced thermoelectric cooling at cold junction interfaces”, *Applied physics letters* **80**, 3006–3008 (2002) (cit. on p. 52).
- [120] R. S. Whitney, “Finding the quantum thermoelectric with maximal efficiency and minimal entropy production at given power output”, *Phys. Rev. B* **91**, 115425 (2015) (cit. on p. 52).
- [121] R. S. Whitney, R. Sánchez, and J. Splettstoesser, “Quantum thermodynamics of nanoscale thermoelectrics and electronic devices”, in *Thermodynamics in the quantum regime* (Springer, 2018), pp. 175–206 (cit. on p. 52).
- [122] M. Josefsson, A. Svilans, A. M. Burke, E. A. Hoffmann, S. Fahlvik, C. Thelander, M. Leijnse, and H. Linke, “A quantum-dot heat engine operating close to the thermodynamic efficiency limits”, *Nat. Nanotechnol.* **13**, 920–924 (2018) (cit. on p. 52).
- [123] A. Svilans, A. M. Burke, S. F. Svensson, M. Leijnse, and H. Linke, “Non-linear thermoelectric response due to energy-dependent transport properties of a quantum dot”, *Physica E* **82**, 34–38 (2016) (cit. on p. 52).
- [124] A. Svilans, M. Leijnse, and H. Linke, “Experiments on the thermoelectric properties of quantum dots”, *C. R. Phys.* **17**, 1096–1108 (2016) (cit. on p. 52).
- [125] D. Sánchez and R. López, “Nonlinear phenomena in quantum thermoelectrics and heat”, *C. R. Phys.* **17**, 1060–1071 (2016) (cit. on p. 52).
- [126] M. Josefsson, A. Svilans, H. Linke, and M. Leijnse, “Optimal power and efficiency of single quantum dot heat engines: Theory and experiment”, *Phys. Rev. B* **99**, 235432 (2019) (cit. on p. 52).
- [127] A. Svilans, M. Leijnse, and H. Linke, “Experiments on the thermoelectric properties of quantum dots”, *Comptes Rendus Physique* **17**, 1096–1108 (2016) (cit. on p. 52).
- [128] J. Prance, C. Smith, J. Griffiths, S. Chorley, D Anderson, G. Jones, I Farrier, and D. Ritchie, “Electronic refrigeration of a two-dimensional electron gas”, *Physical review letters* **102**, 146602 (2009) (cit. on p. 52).

-
- [129] G. D. Mahan and J. O. Sofo, “The best thermoelectric”, *Proc. Natl. Acad. Sci. U.S.A.* **93**, 7436–7439 (1996) (cit. on p. 52).
- [130] T. E. Humphrey, R. Newbury, R. P. Taylor, and H. Linke, “Reversible Quantum Brownian Heat Engines for Electrons”, *Phys. Rev. Lett.* **89**, 116801 (2002) (cit. on p. 52).
- [131] M. S. Dresselhaus, G. Chen, M. Y. Tang, R. G. Yang, H. Lee, D. Z. Wang, Z. F. Ren, J.-P. Fleurial, and P. Gogna, “New Directions for Low-Dimensional Thermoelectric Materials”, *Adv. Mater.* **19**, 1043–1053 (2007) (cit. on p. 52).
- [132] A. Mani and C. Benjamin, “Helical thermoelectrics and refrigeration”, *Phys. Rev. E* **97**, 022114 (2018) (cit. on p. 53).
- [133] A. Mani and C. Benjamin, “Helical thermoelectrics and refrigeration”, *Physical Review E* **97**, 022114 (2018) (cit. on p. 53).
- [134] J. Pendry, “Quantum limits to the flow of information and entropy”, *Journal of Physics A: Mathematical and General* **16**, 2161 (1983) (cit. on p. 53).
- [135] R. S. Whitney, “Finding the quantum thermoelectric with maximal efficiency and minimal entropy production at given power output”, *Physical Review B* **91**, 115425 (2015) (cit. on p. 53).
- [136] L. Molenkamp, T. Gravier, H Van Houten, O. Buijk, M. Mabeoone, and C. Foxon, “Peltier coefficient and thermal conductance of a quantum point contact”, *Physical review letters* **68**, 3765 (1992) (cit. on p. 53).
- [137] S. Jezouin, F. Parmentier, A Anthore, U Gennser, A Cavanna, Y. Jin, and F. Pierre, “Quantum limit of heat flow across a single electronic channel”, *Science* **342**, 601–604 (2013) (cit. on p. 53).
- [138] R. S. Whitney, “Thermodynamic and quantum bounds on nonlinear dc thermoelectric transport”, *Physical Review B* **87**, 115404 (2013) (cit. on p. 53).
- [139] I.-J. Chen, A. Burke, A. Svilans, H. Linke, and C. Thelander, “Thermoelectric power factor limit of a 1D nanowire”, *Physical review letters* **120**, 177703 (2018) (cit. on p. 54).
- [140] H. Thierschmann, R. Sánchez, B. Sothmann, F. Arnold, C. Heyn, W. Hansen, H. Buhmann, and L. W. Molenkamp, “Three-terminal energy harvester with coupled quantum dots”, *Nature nanotechnology* **10**, 854–858 (2015) (cit. on pp. 54, 55).
- [141] C Altimiras, H Le Sueur, U Gennser, A Cavanna, D Mailly, and F Pierre, “Non-equilibrium edge-channel spectroscopy in the integer quantum Hall regime”, *Nature Physics* **6**, 34–39 (2010) (cit. on pp. 54, 55).

-
- [142] O. Abah and E. Lutz, “Efficiency of heat engines coupled to nonequilibrium reservoirs”, *EPL (Europhysics Letters)* **106**, 20001 (2014) (cit. on p. 55).
- [143] W. Niedenzu, D. Gelbwaser-Klimovsky, A. G. Kofman, and G. Kurizki, “On the operation of machines powered by quantum non-thermal baths”, *New Journal of Physics* **18**, 083012 (2016) (cit. on p. 55).
- [144] G. Francica, F. C. Binder, G. Guarnieri, M. T. Mitchison, J. Goold, and F. Plastina, “Quantum Coherence and Ergotropy”, *arXiv* (2020) [10.1103/PhysRevLett.125.180603](https://arxiv.org/abs/10.1103/PhysRevLett.125.180603), eprint: 2006.05424 (cit. on p. 55).
- [145] M. Crosser, J. Huang, F. Pierre, P. Virtanen, T. T. Heikkilä, F. Wilhelm, and N. O. Birge, “Nonequilibrium transport in mesoscopic multi-terminal SNS Josephson junctions”, *Physical Review B* **77**, 014528 (2008) (cit. on p. 55).
- [146] A. Fornieri, G. Timossi, R. Bosisio, P. Solinas, and F. Giazotto, “Negative differential thermal conductance and heat amplification in superconducting hybrid devices”, *Physical Review B* **93**, 134508 (2016) (cit. on p. 56).
- [147] C. W. J. Beenakker, “Random-matrix theory of quantum transport”, *Rev. Mod. Phys.* **69**, 731–808 (1997) (cit. on p. 59).
- [148] F. Hajiloo, F. Hassler, and J. Splettstoesser, “Mesoscopic effects in the heat conductance of superconducting-normal-superconducting and normal-superconducting junctions”, *Physical Review B* **99**, 235422 (2019) (cit. on p. 60).
- [149] F. Hajiloo, P. T. Alonso, N. Dashti, L. Arrachea, and J. Splettstoesser, “Detailed study of nonlinear cooling with two-terminal configurations of topological edge states”, *Phys. Rev. B* **102**, 155434 (2020) (cit. on p. 62).
- [150] F. Hajiloo, R. Sánchez, R. S. Whitney, and J. Splettstoesser, “Quantifying nonequilibrium thermodynamic operations in a multiterminal mesoscopic system”, *Physical Review B* **102**, 155405 (2020) (cit. on p. 64).
- [151] P. Virtanen and F. Giazotto, “Fluctuation of heat current in Josephson junctions”, *AIP Adv.* **5**, 027140 (2015) (cit. on p. 69).
- [152] N. Freitas and M. Esposito, “Characterizing autonomous Maxwell demons”, *arXiv* (2020), eprint: 2011.04497 (cit. on p. 69).